

# HIGH-ORDER METHODS FOR A PRESSURE POISSON EQUATION REFORMULATION OF THE NAVIER-STOKES EQUATIONS WITH ELECTRIC BOUNDARY CONDITIONS

RODOLFO RUBEN ROSALES, BENJAMIN SEIBOLD, DAVID SHIROKOFF, AND DONG ZHOU

**ABSTRACT.** Pressure Poisson equation (PPE) reformulations of the incompressible Navier-Stokes equations (NSE) replace the incompressibility constraint by a Poisson equation for the pressure and a suitable choice of boundary conditions. This yields a time-evolution equation for the velocity field only, with the pressure gradient acting as a nonlocal operator. Thus, numerical methods based on PPE reformulations, in principle, have no limitations in achieving high order. In this paper, it is studied to what extent high-order methods for the NSE can be obtained from a specific PPE reformulation with electric boundary conditions (EBC). To that end, implicit-explicit (IMEX) time-stepping is used to decouple the pressure solve from the velocity update, while avoiding a parabolic time-step restriction; and mixed finite elements are used in space, to capture the structure imposed by the EBC. Via numerical examples, it is demonstrated that the methodology can yield at least third order accuracy in space and time.

## 1. INTRODUCTION

Developing efficient high-order time stepping methods for the incompressible Navier-Stokes equations (NSE) is challenging due to the fact that the velocity and pressure are coupled via an incompressibility constraint. Numerical methods that treat both the velocity  $\mathbf{u}$  and the pressure  $p$  in a fully implicit fashion [43] provide a comparatively straightforward pathway towards high-order. However, fully implicit approaches result in large (possibly nonlinear) saddle-point systems. This imposes a requirement to select spatial discretizations that ensure stable solutions of the resulting discrete equations (i.e. staggered grids [27], or finite elements satisfying the inf-sup condition [19]). In addition, the resulting discrete saddle point problems are non-trivial to solve efficiently [11, 22, 12].

On the other hand, many numerical approaches that decouple  $\mathbf{u}$  and  $p$  result in smaller systems of equations with fewer coupled variables, and often times avoid a saddle-point structure. Hence, such methodologies are attractive for certain large-scale problems. Unfortunately, it is challenging to achieve high-order (in time) when decoupling velocity and pressure. This paper develops finite element approaches for certain pressure Poisson equation (PPE) reformulations of the Navier-Stokes equations that allow for a systematic pathway towards high order while decoupling velocity and pressure.

Numerical methods for the NSE that decouple velocity and pressure date back to the late 1960s with the introduction of projection methods [17, 56]. The idea of projection methods is to first evolve the velocity without the pressure, and then project the velocity back into the space of divergence-free fields via a Poisson problem. Projection methods are one example of a larger class of methods known as fractional step methods [47]. Efforts have been made in the past few decades to improve the accuracy of projection and fractional step methods to second order (in time), and higher, [10, 36, 38, 13]. In particular, accurate methods that go beyond second order are an ongoing area of research [48, 45]. In addition to the difficulties of achieving high order in time accuracy, projection methods carry the risk of producing numerical boundary layers via the Poisson equation for the pressure, which causes a degradation in spatial error convergence. An extensive overview of projection methods is given by Guermond, Mineev, and Shen in [26], where projection methods and various improvements, as well as their theoretical and numerical convergence results are discussed. Recent progress on generalizing the artificial compressibility method [24, 25] (which has traditionally been

---

*Date:* February 25, 2020.

*2000 Mathematics Subject Classification.* 65L06; 65M60; 76D05.

*Key words and phrases.* Incompressible Navier-Stokes; Pressure Poisson equation; Electric boundary conditions; mixed finite elements; IMEX schemes.

first order in time) has lead to alternative avenues that obtain high-order (beyond second order) in time schemes.

PPE reformulations of the Navier-Stokes equations [23, 28, 30, 31, 33, 34, 41, 49, 52, 55, 58] provide an alternate route towards devising high-order in time numerical methods. The basic idea underlying PPE approaches is not to discretize the NSE directly, but instead to (i) reformulate the NSE into a system of PDEs with a Poisson equation for the pressure in lieu of the divergence constraint (the PPE system), (ii) devise boundary conditions that ensure that the new set of equations guarantees incompressibility [23, 36, 28, 52], and then (iii) discretize and solve the resulting PPE system. The solution to the Poisson equation for the pressure is designed so that the PPE reformulation is equivalent to the original NSE for solutions that are sufficiently smooth. In other words, at the continuous level, solving the PPE is equivalent to solving the Navier-Stokes equations. In a sequence of work by Henshaw et al. [28, 29, 30, 31], the recovery of the pressure through the solution of a pressure Poisson problem was done in a discrete setting (with finite differences), using the boundary condition  $\nabla \cdot \mathbf{u} = 0$  together with other numerical boundary conditions. PPE formulations as PDEs were introduced in [34] by Johnston and Liu, and in [55] by Shirokoff and Rosales. Once the PPE has been formulated as a set of continuous PDEs, one may then examine a variety of different numerical discretizations (in both space and time) to solve the PPE system (and hence, equivalently, the NSE).

One important advantage of PPE reformulations compared to the standard form of the NSE is that by solving the Poisson equation, the pressure can be viewed as a global function of the velocity field  $p = P(\mathbf{u})$ . The fact that the pressure can be written as a function of the velocity enables straight-forward numerical approaches for decoupling the velocity and pressure, i.e. to enable implicit-explicit time-stepping strategies. PPE reformulations then provide the possibility to devise high-order in time numerical methods within a systematic framework. Note also that (unlike the NSE) PPE reformulations are defined even if the initial conditions are not incompressible [55, 32], which can be an important advantage when dealing with real data. Drawbacks of PPE reformulations are: (i) For the numerical solution the (numerical) divergence field is not exactly zero. (ii) The pressure boundary conditions are typically complicated. Thus their interaction with the velocity is not straightforward to understand and analyze.

Here we focus on numerical methods based on the Shirokoff-Rosales (SR) PPE reformulation proposed in [55]. Numerical discretizations for the SR PPE reformulation have been proposed in the context of standard finite difference methods [55] and meshfree finite difference method [59]. In [55], a second order finite difference scheme was proposed using a staggered spatial grid and a second order semi-implicit strategy in time where the viscous term was treated implicitly via Crank-Nicolson and the pressure was treated explicitly using a second order Adams-Bashforth method. Curved boundaries were embedded into a Cartesian grid, which could successfully handle irregular domains, but it was cumbersome to implement and did not generalize to arbitrary order. Meshfree finite difference methods for the SR PPE reformulation were devised in [59] as an alternative to allow for the handling of irregular domains (without re-entrant corners). Specifically, [59] devised second order schemes with implicit-explicit time-stepping. Extensions to higher spatial order require larger stencils, thus lead to denser matrices and more costly computations.

In this paper we investigate a finite element discretization for a PPE reformulation with electric boundary conditions motivated by the SR PPE. The approach has the advantage of allowing for a systematic extension to higher spatial order. We also use implicit-explicit (IMEX) time-stepping, specifically IMEX Runge-Kutta (RK) methods that decouple the velocity and the pressure solves. We study the extent to which this yields desirable convergence and stability properties — i.e. better than second order in time, while avoiding a parabolic time step restriction  $\Delta t = O(\Delta x^2)$ . As a final note, we remark that the global existence of weak solutions to the SR PPE reformulation, as well as to the Johnston and Liu [34] PPE reformulation, has been proved [32] for no-slip boundary conditions. The proofs provide appropriate function spaces for the weak solutions, but they do not pursue finite element discretizations of the weak solutions.

This paper is organized as follows. In §2, we introduce a PPE reformulation motivated by the SR PPE of the Navier-Stokes equations. This reformulation uses non-standard boundary conditions for the velocity — i.e. electric boundary conditions (EBC). The resulting vector Poisson-type problem with EBC, when solved with standard nodal FEM, exhibits the Babuška paradox, which can be overcome by using a mixed FEM formulation. In §3, we present a numerical method for the *linear* time-dependent problem (i.e. without the nonlinear advection term), based on mixed FEM and IMEX RK time-stepping. We illustrate, via numerical tests, that the proposed method can achieve (at least) 3rd order in space and in time. In §4, we discuss

how to extend the proposed method to the nonlinear case. Numerical results are shown, for manufactured solutions, as well as for practical benchmark examples (lid-driven cavity, backward-facing step).

## 2. PRESSURE POISSON EQUATION REFORMULATION OF THE NAVIER-STOKES EQUATIONS

In this section, we introduce a pressure Poisson equation reformulation of the Navier-Stokes equations with electric boundary conditions similar to the one proposed in [55]. Consider the time-dependent incompressible Navier-Stokes equations (NSE) in a connected domain  $\Omega \in \mathbb{R}^N$ , where  $N = 2$  or  $3$ , with a piece-wise smooth boundary  $\partial\Omega$ , for domains with Dirichlet boundary data,

$$\begin{aligned} (2.1a) \quad & \mathbf{u}_t + (\mathbf{u} \cdot \nabla)\mathbf{u} = \nu\Delta\mathbf{u} - \nabla p + \mathbf{f} && \text{in } \Omega \times (0, T], \\ (2.1b) \quad & \nabla \cdot \mathbf{u} = 0 && \text{in } \Omega \times (0, T], \\ (2.1c) \quad & \mathbf{u}(\mathbf{x}, t) = \mathbf{g}(\mathbf{x}, t) && \text{on } \partial\Omega \times [0, T], \\ (2.1d) \quad & \mathbf{u}(\mathbf{x}, 0) = \mathbf{u}_0(\mathbf{x}) && \text{in } \Omega, \end{aligned}$$

where  $\nu > 0$  is the kinematic viscosity. Equation (2.1a) follows from the conservation of momentum, and (2.1b) is conservation of mass. Furthermore, we impose the following compatibility conditions:

$$(2.2) \quad \text{Continuity between the initial and the boundary conditions: } \mathbf{u}_0(\mathbf{x}) = \mathbf{g}(\mathbf{x}, 0) \text{ on } \partial\Omega.$$

$$(2.3) \quad \text{Incompressibility of the initial condition: } \nabla \cdot \mathbf{u}_0 = 0 \text{ in } \Omega.$$

$$(2.4) \quad \text{Zero net flux through the boundary: } \int_{\partial\Omega} \mathbf{n} \cdot \mathbf{g} \, dS = 0.$$

For the numerical solution of (2.1) we will instead solve a PPE reformulation, whose fundamental difference from previously proposed PPE reformulations lies in the velocity boundary conditions: incompressibility and the tangential flow are prescribed at the boundary. Further, the normal velocity is enforced via a relaxation term in the pressure equation. The PPE reformulation reads as follows

$$\begin{aligned} (2.5a) \quad & \mathbf{u}_t + (\mathbf{u} \cdot \nabla)\mathbf{u} = \nu\Delta\mathbf{u} - \nabla P(\mathbf{u}) + \mathbf{f} && \text{in } \Omega \times (0, T], \\ (2.5b) \quad & \mathbf{n} \times \mathbf{u} = \mathbf{n} \times \mathbf{g} && \text{on } \partial\Omega \times [0, T], \\ (2.5c) \quad & \nabla \cdot \mathbf{u} = 0 && \text{on } \partial\Omega \times [0, T]. \end{aligned}$$

Here  $P(\mathbf{u})$  is the solution to the pressure Poisson equation (in a slight abuse of notation, we use both  $p$  and  $P(\mathbf{u})$  for the pressure)

$$\begin{aligned} (2.6a) \quad & \Delta p = \nabla \cdot (\mathbf{f} - (\mathbf{u} \cdot \nabla)\mathbf{u}) && \text{in } \Omega, \\ (2.6b) \quad & \frac{\partial p}{\partial \mathbf{n}} = \mathbf{n} \cdot (\mathbf{f} - \mathbf{g}_t - \nu\nabla \times \nabla \times \mathbf{u} - (\mathbf{u} \cdot \nabla)\mathbf{u}) + \lambda \mathbf{n} \cdot (\mathbf{u} - \mathbf{g}) && \text{on } \partial\Omega. \end{aligned}$$

The term  $\lambda \mathbf{n} \cdot (\mathbf{u} - \mathbf{g})$ , where  $\lambda > 0$  is a constant, is a relaxation term that guarantees that the normal velocity condition at the boundary  $\partial\Omega$  is exponentially attracting — see equation (2.8).

The tangential boundary conditions, together with the divergence-free boundary condition in (2.5), often appear in electrostatics as “electric boundary conditions” (EBC). We adopt this terminology in this paper. The PPE system (2.5–2.6) is almost identical to the one introduced in [55], the difference being here that  $\mathbf{n} \cdot \nabla \times \nabla \times \mathbf{u}$  appears in the boundary condition for  $p$  in lieu of  $\mathbf{n} \cdot \Delta\mathbf{u}$  (which appeared in [55]). The choice of  $\mathbf{n} \cdot \nabla \times \nabla \times \mathbf{u}$  in the pressure boundary condition is done to yield a simpler finite element discretization for the pressure than  $\mathbf{n} \cdot \Delta\mathbf{u}$ . Note that the pressure boundary condition  $\mathbf{n} \cdot \nabla \times \nabla \times \mathbf{u}$  has appeared in several projection method and PPE formulations with Dirichlet boundary conditions for the velocity such as [36, 34, 45]. We re-emphasize that our goal is to examine PPE schemes with EBC in the velocity.

In previous works, the PPE systems in [55] and [34] were shown to be, for sufficiently smooth (up to the boundary) solutions  $(\mathbf{u}, p)$ , equivalent to the NSE (2.1). It is relatively straightforward to show that smooth solutions to the NSE solve (2.5–2.6) and hence the PPE system contains the NSE solutions. We now show that solutions to the PPE system (2.5–2.6) solve the NSE — the approach follows closely to [55, 34] with a minor difference due to the combination of the EBC for the velocity and  $\mathbf{n} \cdot \nabla \times \nabla \times \mathbf{u}$  boundary condition for the pressure.

Assume that  $(\mathbf{u}, p)$  is a smooth solution to (2.5–2.6). Then the PPE reformulation recovers the incompressibility constraint: apply the divergence to the momentum equation (2.5a) and substitute into (2.6a).

This yields the heat equation for the divergence  $\phi = \nabla \cdot \mathbf{u}$ , with homogeneous Dirichlet boundary conditions due to (2.5c). That is:

$$(2.7) \quad \begin{cases} \phi_t = \nu \Delta \phi & \text{in } \Omega, \\ \phi = 0 & \text{on } \partial\Omega. \end{cases}$$

Therefore, if  $\phi(t=0) = \nabla \cdot \mathbf{u}_0 = 0$ , then  $\phi = 0$  for all time, and  $\mathbf{u}$  is incompressible. If, due to numerical approximation errors, the velocity field starts to depart from the  $\nabla \cdot \mathbf{u} = 0$  subspace, the heat equation dynamics ensure that  $\mathbf{u}$  is driven back towards incompressibility. This property indicates that there is no need to impose a discrete incompressibility principle in PPE reformulations, thus providing more flexibility in the design of numerical approximation methods.

Secondly, the PPE ensures that the normal velocity at the boundary, i.e.  $\mathbf{n} \cdot \mathbf{u} = \mathbf{n} \cdot \mathbf{g}$ , is enforced implicitly through the ordinary differential equation

$$(2.8) \quad \begin{cases} \mathbf{n} \cdot (\mathbf{u}_t - \mathbf{g}_t) = \nu \mathbf{n} \cdot \nabla \phi - \lambda \mathbf{n} \cdot (\mathbf{u} - \mathbf{g}) & \text{on } \partial\Omega \times (0, T], \\ \mathbf{n} \cdot (\mathbf{u} - \mathbf{g})|_{\partial\Omega} = 0 & \text{at } t = 0, \end{cases}$$

which is obtained by evaluating the normal component of the momentum equation (2.5a) at the boundary, and using the pressure boundary condition (2.6b) along with the identity that  $\Delta \mathbf{u} = \nabla(\nabla \cdot \mathbf{u}) - \nabla \times \nabla \times \mathbf{u}$ . By virtue of equation (2.7), we have that  $\phi = 0$ , so that (2.8) reduces to a simple ODE at every point  $\mathbf{x} \in \partial\Omega$ :  $\dot{\alpha} = -\lambda \alpha$  where  $\alpha = \mathbf{n} \cdot (\mathbf{u} - \mathbf{g})$ . Hence,  $\mathbf{n} \cdot \mathbf{u} = \mathbf{n} \cdot \mathbf{g}$  for all time. In the presence of numerical approximation errors, the term  $-\lambda \mathbf{n} \cdot (\mathbf{u} - \mathbf{g})$  adds an exponential decay to the error in the normal velocity on the domain boundary.

Note that in the absence of the  $\lambda$ -term, the exact solution to equation (2.8) still satisfies  $\mathbf{n} \cdot (\mathbf{u} - \mathbf{g}) = 0$ . However, in practice, numerical errors may result in a drift of the normal velocity [55], which requires stabilization via the  $\lambda$ -term. Moreover, for the steady state system, the condition  $\lambda > 0$  is required for a unique solution.

**Remark 2.1** (Solvability condition for the pressure Poisson equation). *A solvability condition is required in order for the pressure Poisson equation (2.6) to have a solution, that is:*

$$(2.9) \quad \int_{\Omega} -\nu \nabla \cdot (\nabla \times \nabla \times \mathbf{u}) + \lambda \nabla \cdot \mathbf{u} \, dV - \int_{\partial\Omega} \mathbf{n} \cdot \mathbf{g}_t + \lambda \mathbf{n} \cdot \mathbf{g} \, dS = 0.$$

*The incompressibility condition  $\nabla \cdot \mathbf{u} = 0$  and the zero net flux condition (2.4) ensure that both the volume integral and the boundary integral in equation (2.9) vanish. However, numerical approximation errors in the discrete Poisson equation may result in schemes that do not exactly satisfy the discrete version of the solvability condition (2.9). Whenever this occurs, the discrete Poisson equation must be solved in the least squares sense. This is achieved by formulating an augmented system that projects the right hand side of the pressure Poisson problem onto one for which the solvability condition is satisfied, see §A.*

**Remark 2.2.** *There is a rich variety of possible PPE reformulations. At the continuum level, one can add  $\nabla \cdot \mathbf{u}$  anywhere (because  $\nabla \cdot \mathbf{u} = 0$ ), as long as the resulting systems are well-posed and are equivalent to the original problem. However, in the presence of approximation errors, one generally has  $\nabla \cdot \mathbf{u}_h \neq 0$ , thus adding  $\nabla \cdot \mathbf{u}$  will lead to different numerical schemes. For example, Henshaw and Petersson [31] add a divergence damping term  $\delta \nabla \cdot \mathbf{u}$ , with  $\delta \geq 0$ , to the pressure Poisson equation to obtain*

$$\Delta p = \nabla \cdot (\mathbf{f} - (\mathbf{u} \cdot \nabla) \mathbf{u}) + \delta \nabla \cdot \mathbf{u}.$$

*With this, the divergence satisfies the PDE  $\phi_t = \Delta \phi - \delta \phi$ . In the discretized case, where the divergence is not exactly zero, the damping term adds an exponential decay that can further help keeping the discrete divergence small.*

### 3. NUMERICAL METHOD FOR THE TIME-DEPENDENT STOKES PROBLEM

In this section, we present a numerical method for the PPE reformulation (2.5–2.6) of the time-dependent Stokes equation

$$(3.1) \quad \mathbf{u}_t = \nu \Delta \mathbf{u} - \nabla P(\mathbf{u}) + \mathbf{f} \quad \text{in } \Omega \times (0, T], \quad \mathbf{n} \times \mathbf{u} = \mathbf{n} \times \mathbf{g} \text{ and } \nabla \cdot \mathbf{u} = 0 \quad \text{on } \partial\Omega \times [0, T],$$

where  $P(\mathbf{u})$  solves the pressure Poisson equation

$$(3.2) \quad \Delta p = \nabla \cdot \mathbf{f} \quad \text{in } \Omega, \quad \frac{\partial p}{\partial \mathbf{n}} = \mathbf{n} \cdot (\mathbf{f} - \mathbf{g}_t - \nu \nabla \times \nabla \times \mathbf{u}) + \lambda \mathbf{n} \cdot (\mathbf{u} - \mathbf{g}) \quad \text{on } \partial\Omega.$$

To handle irregular domains we adopt a mixed finite element method (FEM) for the spatial discretizations of  $\mathbf{u}$  (see §3.1), and nodal FEM for  $p$  (see §3.2). Note that the motivation for adopting a mixed FEM for  $\mathbf{u}$  is to address structural issues (discussed below) that arise from the electric boundary conditions (EBC) in the momentum equation. Unlike mixed approaches for the Stokes/Navier-Stokes equations in which the elements approximating  $\mathbf{u}$  and  $p$  need to satisfy a discrete inf-sup condition [19, 44], the mixed formulation employed here is solely for the velocity, and the nodal elements for the pressure do not need to satisfy an inf-sup condition with the velocity elements. For the time evolution (see §3.3), we adopt an implicit-explicit (IMEX) Runge-Kutta (RK) scheme that (due to the PPE formulation) leads to natural approaches for decoupling the velocity  $\mathbf{u}$  from the pressure  $p$ . That is, we treat the viscous term  $\Delta \mathbf{u}$  implicitly and the pressure term  $\nabla p$  explicitly. We carry out convergence studies via the method of manufactured solutions in §3.4.

**3.1. Discretization of the Velocity via Mixed Finite Elements.** In this section we outline the spatial discretization of the velocity via mixed finite elements [19]. The choice of a mixed FEM over other element choices (such as nodal FEM) is due to the EBC in the momentum equation. To be precise, nodal FEM for problems involving electric boundary conditions may converge to the wrong solution, see Remark 3.1. In contrast, mixed FE provide a natural way to handle the EBC.

The mixed formulation presented in this paper is applied to the discretization of the momentum equation (2.5) only, and introduced to handle the EBC by introducing the vorticity  $\sigma = \nabla \times \mathbf{u}$  as a new variable. Hence, there is no inf-sup condition for  $(\mathbf{u}, p)$ , but instead, an inf-sup condition for the velocity and vorticity  $(\mathbf{u}, \sigma)$ . Using the vector identity  $\Delta \mathbf{u} = \nabla(\nabla \cdot \mathbf{u}) - \nabla \times \nabla \times \mathbf{u}$ , and introducing the new variable  $\sigma = \nabla \times \mathbf{u}$  (cf. [3, 2]), equation (3.1) in the PPE reformulation can be recast as:

$$(3.3a) \quad \sigma = \nabla \times \mathbf{u} \quad \text{in } \Omega,$$

$$(3.3b) \quad \mathbf{u}_t = \nu(\nabla(\nabla \cdot \mathbf{u}) - \nabla \times \sigma) - \nabla P(\mathbf{u}) + \mathbf{f} \quad \text{in } \Omega,$$

$$(3.3c) \quad \mathbf{n} \times \mathbf{u} = \mathbf{n} \times \mathbf{g} \quad \text{on } \partial\Omega,$$

$$(3.3d) \quad \nabla \cdot \mathbf{u} = 0 \quad \text{on } \partial\Omega.$$

To obtain the weak formulation of the equations (3.3), we use the spaces

$$H(\text{curl}; \Omega) = \left\{ \mathbf{u} \in L^2(\Omega)^N : \nabla \times \mathbf{u} \in L^2(\Omega)^{N'} \right\},$$

$$H(\text{div}; \Omega) = \left\{ \mathbf{u} \in L^2(\Omega)^N : \nabla \cdot \mathbf{u} \in L^2(\Omega) \right\},$$

with  $N' = 1$  for  $N = 2$  and  $N' = 3$  for  $N = 3$ . We then multiply (3.3a) by a test function  $\tau$  and (3.3b) by a test function  $\mathbf{v}$ , and then apply the integral identities

$$\langle \nabla \times \mathbf{u}, \tau \rangle = \langle \mathbf{u}, \nabla \times \tau \rangle + \int_{\partial\Omega} \tau \cdot (\mathbf{n} \times \mathbf{u}) \, dS,$$

$$\langle \nabla \times \sigma - \nabla(\nabla \cdot \mathbf{u}), \mathbf{v} \rangle = \langle \nabla \times \sigma, \mathbf{v} \rangle + \langle \nabla \cdot \mathbf{u}, \nabla \cdot \mathbf{v} \rangle - \int_{\partial\Omega} (\nabla \cdot \mathbf{u})(\mathbf{v} \cdot \mathbf{n}) \, dS,$$

along with the tangential boundary condition (3.3c) and the divergence-free boundary condition (3.3d). This procedure yields the following mixed formulation for (3.3): Find  $\sigma \in X$ ,  $\mathbf{u} \in H(\text{div}; \Omega)$  such that

$$(3.4a) \quad \langle \sigma, \tau \rangle - \langle \mathbf{u}, \nabla \times \tau \rangle = \int_{\partial\Omega} \tau \cdot (\mathbf{n} \times \mathbf{g}) \, dS \quad \forall \tau \in X,$$

$$(3.4b) \quad \langle \mathbf{u}_t, \mathbf{v} \rangle + \nu \langle \nabla \times \sigma, \mathbf{v} \rangle + \nu \langle \nabla \cdot \mathbf{u}, \nabla \cdot \mathbf{v} \rangle = \langle \mathbf{f} - \nabla P(\mathbf{u}), \mathbf{v} \rangle \quad \forall \mathbf{v} \in H(\text{div}; \Omega).$$

Here  $X = H^1(\Omega)$  when  $N = 2$  and  $X = H(\text{curl}; \Omega)$  when  $N = 3$ . Notice that both the tangential boundary condition and the divergence boundary condition from (2.5) appear in the weak form (3.4) as natural boundary conditions (the spaces of functions  $X$  and  $H(\text{div}; \Omega)$  do not enforce the boundary conditions).

Let  $\Sigma^h$  and  $V^h$  be finite dimensional subspaces for  $X$  and  $H(\text{div}; \Omega)$  respectively. The semi-discrete mixed formulation of (3.4) is as follows: Find  $(\sigma_h, \mathbf{u}_h) \in \Sigma^h \times V^h$  such that  $\mathbf{u}_h(t=0) = \mathbf{u}_{0h}$  and

$$(3.5a) \quad \langle \sigma_h, \tau_h \rangle - \langle \mathbf{u}_h, \nabla \times \tau_h \rangle = \int_{\partial\Omega} \tau_h(\mathbf{n} \times \mathbf{g}) \, dS \quad \forall \tau \in \Sigma^h$$

$$(3.5b) \quad \langle (\mathbf{u}_h)_t, \mathbf{v}_h \rangle = -\nu \langle \nabla \cdot \mathbf{u}_h, \nabla \cdot \mathbf{v}_h \rangle - \nu \langle \nabla \times \sigma_h, \mathbf{v}_h \rangle + \langle \mathbf{f} - \nabla P(\mathbf{u}_h), \mathbf{v}_h \rangle \quad \forall \mathbf{v}_h \in V^h$$

where  $\mathbf{u}_{0h}$  is the projection of the initial condition  $\mathbf{u}_0$  onto the space  $V^h$ , and  $P(\mathbf{u}_h)$  is the solution to the discretized pressure Poisson problem using the velocity approximation (see §3.2).

There are different stable pairs of finite elements for the spaces  $\Sigma^h$  and  $V^h$  [3, 4, 5]. Here in the case of  $N = 2$ , we choose nodal finite elements (Lagrange finite elements  $P_r$ ) of degree  $r \geq 1$  for  $\sigma_h$  and Raviart-Thomas elements ( $RT_{r-1}$ ) of the same degree for the vector field  $\mathbf{u}_h$ . That is

$$\Sigma^h \times V^h = P_r \times RT_{r-1} \quad \text{for } r \geq 1.$$

In the 3-dimensional case, the corresponding space for  $\sigma$  is  $H(\text{curl}; \Omega)$ , and Nédélec elements ( $NED_r^1$ ) are used.

**Remark 3.1.** (*Failure of nodal FEM*) Nodal FEM may fail to converge to the true solution for EBC problems, for two different reasons: (i) the Babuška paradox [9, 8], and (ii) the inability to approximate singularities in the solution, such as those caused by re-entrant corners in the domain. The Babuška paradox [9, 8] occurs when FEM solutions on polygonal approximations of domains with curved boundaries converge to a function (as the mesh size goes to zero) that is not the solution of the underlying continuum problem. For instance, the vector Laplace problem (with  $\nabla \cdot \mathbf{f} = 0$ )

$$(3.6) \quad \Delta \mathbf{u} = \mathbf{f} \quad \text{in } \Omega, \quad \text{with b.c.} \quad \nabla \cdot \mathbf{u} = 0 \quad \text{and} \quad \mathbf{n} \times \mathbf{u} = 0 \quad \text{on } \partial\Omega,$$

has the weak formulation: Given  $\mathbf{f} \in L^2(\Omega)^N$ ,  $\nabla \cdot \mathbf{f} = 0$ , find  $\mathbf{u} \in V$ , such that for every  $\mathbf{v} \in V$

$$(3.7) \quad \langle \nabla \times \mathbf{u}, \nabla \times \mathbf{v} \rangle + \langle \nabla \cdot \mathbf{u}, \nabla \cdot \mathbf{v} \rangle = \langle \mathbf{f}, \mathbf{v} \rangle.$$

Nodal FEM approximations based on  $V = H_{0t}^1(\Omega)^N = \{\mathbf{u} \in H^1(\Omega)^N : \mathbf{n} \times \mathbf{u}|_{\partial\Omega} = 0\}$  exhibit the Babuška paradox and may not converge to the solution of (3.6) [59].

The second issue with nodal elements is an approximation theory result. The weak formulation (3.7) is uniquely solvable for the following two choices of space:  $V = H_{0t}^1(\Omega)^N$  or  $V = H_0(\text{curl}; \Omega) \cap H(\text{div}; \Omega) = \{\mathbf{u} \in L^2(\Omega)^N : \nabla \cdot \mathbf{u} \in L^2(\Omega)^N, \nabla \times \mathbf{u} \in L^2(\Omega)^{N'}, \mathbf{n} \times \mathbf{u}|_{\partial\Omega} = 0\}$ . When the domain  $\Omega$  is convex or has a globally  $C^2$  boundary, then  $H_{0t}^1(\Omega)^N = H_0(\text{curl}; \Omega) \cap H(\text{div}; \Omega)$  and the solution is divergence-free. When  $\Omega$  has re-entrant corners, we have  $H_{0t}^1(\Omega)^N \subsetneq H_0(\text{curl}; \Omega) \cap H(\text{div}; \Omega)$  and the divergence-free solution may not be in  $H_{0t}^1(\Omega)^N$  [35]. Hence, in general  $H^1$  nodal FEM is not guaranteed to converge to the divergence-free solution.

**3.2. Discretization of the Pressure.** The pressure  $p$  satisfies a Poisson problem with Neumann boundary condition (3.2). Therefore, given the velocity, standard nodal-based finite elements can be used to discretize the pressure Poisson equation. Following the usual procedure for deriving weak formulations, we multiply equation (3.2) by a test function  $q \in H^1(\Omega)$  and apply integration by parts to obtain

$$\langle \nabla p, \nabla q \rangle = \langle \mathbf{f}, \nabla q \rangle - \nu \int_{\partial\Omega} (\mathbf{n} \cdot \nabla \times \nabla \times \mathbf{u}) q \, dS + \lambda \int_{\partial\Omega} \mathbf{n} \cdot (\mathbf{u} - \mathbf{g}) q \, dS - \int_{\partial\Omega} (\mathbf{n} \cdot \mathbf{g}_t) q \, dS.$$

We further substitute  $\sigma = \nabla \times \mathbf{u}$ , which gives rise to two possible different weak formulations for the pressure Poisson equation:

(1) Choosing the boundary integral that involves  $\mathbf{n} \cdot (\nabla \times \sigma)$  yields the first weak formulation

$$(3.8) \quad \langle \nabla p, \nabla q \rangle = \langle \mathbf{f}, \nabla q \rangle - \nu \int_{\partial\Omega} \mathbf{n} \cdot (\nabla \times \sigma) q \, dS + \lambda \int_{\partial\Omega} \mathbf{n} \cdot (\mathbf{u} - \mathbf{g}) q \, dS - \int_{\partial\Omega} (\mathbf{n} \cdot \mathbf{g}_t) q \, dS, \quad \forall q \in H^1(\Omega).$$

(2) Choosing the volume integral of  $(\nabla \times \sigma) \cdot \nabla q$  gives the second weak formulation

$$(3.9) \quad \langle \nabla p, \nabla q \rangle = \langle \mathbf{f}, \nabla q \rangle - \nu \langle \nabla \times \sigma, \nabla q \rangle + \lambda \int_{\partial\Omega} \mathbf{n} \cdot (\mathbf{u} - \mathbf{g}) q \, dS - \int_{\partial\Omega} (\mathbf{n} \cdot \mathbf{g}_t) q \, dS, \quad \forall q \in H^1(\Omega).$$

In numerical tests both choices return almost identical results. Therefore in this paper we show only the results of numerical experiments conducted with the first formulation, (3.8).

**3.3. Time-stepping via IMEX Schemes.** One advantage of the PPE reformulation is that the pressure appears as a global function of the velocity in the momentum equation. This enables conceptually straightforward implicit-explicit (IMEX) time discretizations of the PPE system that treat the pressure explicitly and viscosity implicitly. An implicit treatment of the viscosity term is desirable for low to moderate Reynolds numbers as to avoid a parabolic time step stability restriction. In addition, an explicit treatment of the pressure is desirable to avoid solving large coupled systems involving  $(p, \mathbf{u})$ .

IMEX schemes are based on an additive splitting of an ODE that take the following form:

$$(3.10) \quad \frac{du}{dt} = f(u) + g(u).$$

Popular IMEX methods are linear multistep IMEX schemes [6] and IMEX Runge-Kutta (RK) methods [7]. Here we focus on IMEX RK schemes because they have less restrictive stability properties than IMEX multistep methods. We consider IMEX RK schemes that combine two different Runge-Kutta schemes: an explicit RK (ERK) method for  $f(u)$ , and a diagonally implicit RK (DIRK) method for  $g(u)$ . Let  $A \in \mathbb{R}^{s \times s}$ ,  $\mathbf{b}, \mathbf{c} \in \mathbb{R}^s$  be the coefficients of an  $s$ -stage DIRK scheme, and  $\hat{A} \in \mathbb{R}^{(s+1) \times (s+1)}$ ,  $\hat{\mathbf{b}}, \hat{\mathbf{c}} \in \mathbb{R}^{s+1}$  be the coefficients of an  $(s+1)$ -stage ERK scheme with  $\hat{\mathbf{c}}^T = (0, \mathbf{c}^T)$  in the Butcher notation [14], i.e.

$$\frac{\mathbf{c}}{\mathbf{b}^T} \Big| \begin{array}{c} A \\ \hline \end{array} = \begin{array}{c|ccc} c_1 & a_{11} & & \\ c_2 & a_{21} & a_{22} & \\ \vdots & \vdots & \vdots & \ddots \\ c_s & a_{s1} & a_{s2} & \cdots & a_{ss} \\ \hline & b_1 & b_2 & \cdots & b_s \end{array} \quad \frac{\hat{\mathbf{c}}}{\hat{\mathbf{b}}^T} \Big| \begin{array}{c} \hat{A} \\ \hline \end{array} = \begin{array}{c|cccc} 0 & 0 & & & \\ c_1 & \hat{a}_{21} & 0 & & \\ c_2 & \hat{a}_{31} & \hat{a}_{32} & 0 & \\ \vdots & \vdots & \vdots & \vdots & \ddots \\ c_s & \hat{a}_{s+1,1} & \hat{a}_{s+1,2} & \hat{a}_{s+1,3} & \cdots & 0 \\ \hline & \hat{b}_1 & \hat{b}_2 & \hat{b}_3 & \cdots & \hat{b}_{s+1} \end{array}$$

One step of an IMEX scheme from time  $t_n$  to  $t_{n+1} = t_n + \Delta t$  for the splitting (3.10) can be written as follows:

$$\begin{aligned} u^{(i)} &= u^n + \Delta t \sum_{j=1}^i a_{ij} g(u^{(j)}) + \Delta t \sum_{j=1}^i \hat{a}_{i+1,j} f(u^{(j-1)}) \quad \text{for } i = 1, \dots, s \\ u^{n+1} &= u^n + \Delta t \sum_{i=1}^s b_i g(u^{(i)}) + \Delta t \sum_{j=1}^{s+1} \hat{b}_j f(u^{(j-1)}) \end{aligned}$$

where  $u^{(0)} = u^n$ .

**Stability of IMEX RK Schemes for the PPE Reformulation.** IMEX schemes applied to the PPE system (2.5–2.6) may encounter subtle stability issues, and addressing these issues will guide our choice of IMEX time stepping coefficients. First we will examine the numerical stability of an IMEX RK scheme applied to a scalar ODE model for the PPE system (3.1–3.2). The model problem will then yield a stability criterion, which will dictate our choice of IMEX coefficients.

Using the vector identity  $\Delta = \nabla(\nabla \cdot) - \nabla \times \nabla \times$ , and introducing  $\mathcal{A} := -\nabla \times \nabla \times$ , the PPE system (3.1–3.2) can be (exactly) recast (with  $\nu = 1$ , when  $\mathbf{f} = 0$ ,  $\mathbf{g} = 0$ ) as the following non-local evolution

$$(3.11) \quad \mathbf{u}_t = \nabla(\nabla \cdot \mathbf{u}) + \mathcal{A}\mathbf{u} - \mathcal{P}(\mathcal{A}\mathbf{u}) - \lambda \mathcal{P}\mathbf{u} \quad \text{in } \Omega \quad \text{with b.c. } \mathbf{n} \times \mathbf{u} = 0, \quad \nabla \cdot \mathbf{u} = 0 \quad \text{on } \partial\Omega.$$

Here the operator  $\mathcal{P}$  is defined by

$$(3.12) \quad \mathcal{P}\mathbf{w} = \nabla p,$$

where  $p$  solves the Poisson equation

$$(3.13) \quad \Delta p = 0 \quad \text{in } \Omega, \quad \text{with b.c. } \frac{\partial p}{\partial \mathbf{n}} = \mathbf{n} \cdot \mathbf{w} - \bar{w} \quad \text{on } \partial\Omega, \quad \text{where } \bar{w} := \frac{1}{|\partial\Omega|} \int_{\partial\Omega} \mathbf{n} \cdot \mathbf{w} \, dS.$$

By definition,  $\mathcal{P}\mathbf{w}$  generates a divergence-free field, with normal component  $\mathbf{n} \cdot \mathbf{w} - \bar{w}$  at the boundary. It follows that  $\mathcal{P}^2 = \mathcal{P}$ , i.e.  $\mathcal{P}$  is a projection.

The IMEX discretization of (3.11) then treats  $\nabla(\nabla \cdot \mathbf{u}) + \mathcal{A}\mathbf{u}$  implicitly and  $-\mathcal{P}(\mathcal{A}\mathbf{u}) - \lambda \mathcal{P}\mathbf{u}$  explicitly. Due to the structure of the projection,  $\mathcal{P}(\mathcal{A}\mathbf{u})$  is stiff since  $\mathcal{A}$  has two spatial derivatives (i.e. may incur a parabolic time step restriction). Thus both the implicit term (which includes  $\mathcal{A}\mathbf{u}$ ) and the explicit term



Note that the explicit RK scheme  $(\hat{A}, \hat{\mathbf{b}}, \hat{\mathbf{c}})$  is a 4-stage scheme recast as a 5-stage scheme which is stiffly accurate (the last row of  $\hat{A}$  equals the vector  $\hat{\mathbf{b}}^T$ ). This scheme is suitable for the PPE reformulation as it is unconditionally stable when solving the linear model problem (3.14) (see the left panel in Figure 1 for the stability region). We therefore adopt the 3rd order IMEX RK scheme (3.20) for all numerical computations in this paper.

We are unaware of any existing 4th order (or higher) schemes that satisfy the wedge property. For instance, two popular 4th order IMEX RK schemes, one by Cavaglieri and Bewley [16] and the other by Kennedy and Carpenter [37], both violate the wedge property (see Figure 1 middle and right panels).

Note that the wedge property is only a sufficient condition for unconditional stability of the IMEX RK scheme for the model problem (3.14). Nevertheless, this condition can provide insight into the stability property of a given IMEX RK scheme for the PPE reformulation (2.5–2.6). For instance, we generally observe that 4th order schemes violating the wedge property require a stiff parabolic time step restriction  $\Delta t = O(\Delta x^2)$ .

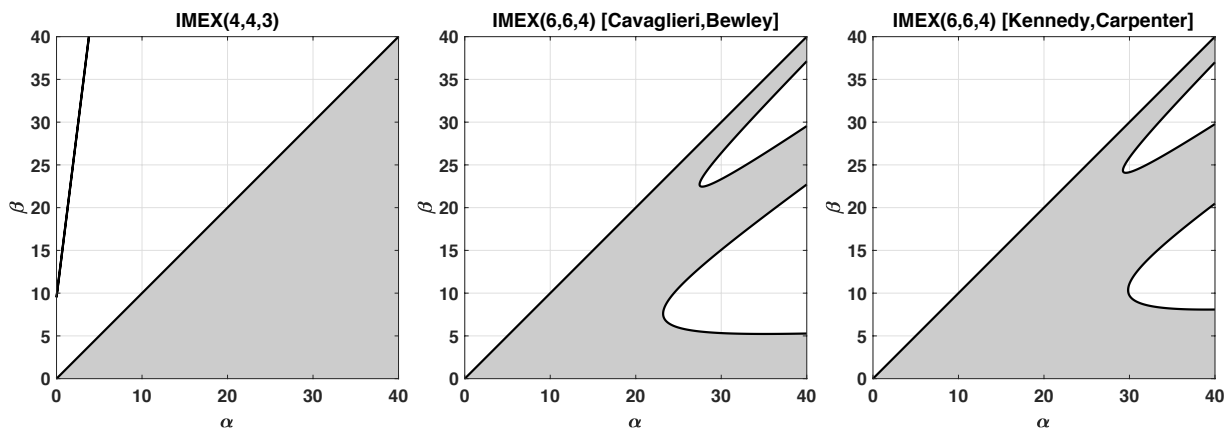


FIGURE 1. Stability regions of three IMEX RK schemes for the scalar test problem  $u_t = -\gamma u + \mu u$ . Left to right: 3rd order IMEX(4,4,3); 4th order IMEX RK scheme by Cavaglieri and Bewley [16]; 4th order IMEX RK scheme by Kennedy and Carpenter [37].

As a final comment on the RK time discretization, RK schemes (including IMEX RK schemes) suffer from order reduction when applied to initial boundary value problems with time-dependent boundary conditions or forcings on the boundary [53, 57, 15]. We summarize the order reduction phenomena in the following remark.

**Remark 3.2.** *Order reduction is a generic problem of RK schemes where the observed temporal convergence rate is lower than the formal order of the scheme. Order reduction is often due to the formation of numerical boundary layers, caused by enforcing boundary conditions in the RK scheme [51]. While several approaches exist to remedy order reduction [15, 1, 51, 37], they do not easily generalize to PPE reformulations or IMEX settings.*

To investigate the high order accuracy of the methods presented in this paper, we choose specific test problems (below) in which the structure of the problem does not lead to order reduction. Because order reduction is a generic phenomenon that is not specific to PPE reformulations, the (important) question of how to avoid order reduction is of generic nature and not specific to this work.

It is worth pointing out that IMEX multistep methods are devoid of order reduction. A key obstacle to the applicability of multistep methods has been their restrictive stability properties, particularly for problems in which the implicit and explicit parts are both stiff [54], such as PPE reformulations. However, recently proposed IMEX multistep methods [50] can achieve unconditional stability for such problems, and thus may provide an alternative suitable time-stepping strategy for PPE reformulations.

**3.4. Numerical Results for Manufactured Solutions.** The goal of this subsection is to demonstrate via numerical examples that, for the time-dependent Stokes problem (3.1–3.2), the proposed method can achieve high-order in space and third order in time. We employ the method of manufactured solutions and

conduct convergence studies for the spatial accuracy (see §3.4.2), the temporal accuracy for the 3rd order IMEX(4,4,3) scheme (3.20) (see §3.4.3), and the accuracy of the overall scheme (see §3.4.4).

We implement the numerical methods using the software package FEniCS [46], which contains an extensive library of finite elements through one of its components: Finite element Automatic Tabulator (FIAT) [39, 40]. It provides  $H(\text{div})$  element spaces such as Raviart-Thomas (RT) elements and  $H(\text{curl})$  elements of the Nédélec types. The triangular meshes used for the computations are generated by the software package Gmsh [20].

**3.4.1. Numerical Results for the Vector Heat Equation with EBC.** Before presenting the results for the PPE reformulation, we show the convergence results for the vector heat equation (VHE) with EBC as a benchmark. This provides both: a baseline for the PPE reformulation convergence study, and a verification of the code. Let the problem domain be  $\Omega = [0, 1] \times [0, 1]$  with periodic b.c. applied in the  $x$ -direction and EBC in the  $y$ -direction. Hence, the problem reads as

$$(3.21a) \quad \mathbf{u}_t = \Delta \mathbf{u} + \mathbf{f} \quad \text{for } (x, y) \in (0, 1)^2,$$

$$(3.21b) \quad \mathbf{n} \times \mathbf{u} = 0, \quad \nabla \cdot \mathbf{u} = 0 \quad \text{for } (x, y) \in [0, 1] \times \{0, 1\},$$

$$(3.21c) \quad \mathbf{u}(0, y) = \mathbf{u}(1, y) \quad \text{for } 0 < y < 1.$$

The divergence-free manufactured solution  $\mathbf{u} = (u, v)^T = (\psi_y, -\psi_x)^T$  is generated by the stream function

$$\psi(x, y, t) = \cos(t) \sin(4\pi(x + y))(4y(1 - y))^4.$$

The manufactured solution is selected so that the velocity field and its derivatives up to certain order vanish at the boundary to suppress the effect of order reduction due to the IMEX RK time-stepping (Remark 3.2).

To conduct a spatial convergence study we use a series of regular meshes with total number of elements 64, 256, 1024, 4096, and 16384. For the time evolution we use the third order IMEX (4,4,3) scheme with a fixed small time step  $\Delta t = 10^{-5}$  (so that the error due to the time-stepping is negligible) and a fixed final time  $T = 10^{-3}$  (100 time steps). The FE spaces are chosen to be  $(\sigma_h, \mathbf{u}_h) \in P_r \times RT_{r-1}$ , with degrees  $r = 1, 2, 3, 4, 5$ . The observed spatial rates of convergence in the  $L^2$  norm are shown in Table 1 (the same rates are observed in the  $L^\infty$  norm). These results confirm the error estimate for the semi-discrete (in space) VHE in [2] where the quantities  $\mathbf{u}$ ,  $\nabla \cdot \mathbf{u}$ ,  $\sigma$  and  $\nabla \times \sigma$  were proved to be at least  $r$ -th order convergent for  $r$ -th order finite elements.

The observed convergence rates are clean, with the exception of  $r = 4$  which shows some degradation in the convergence of  $\nabla \cdot \mathbf{u}$ . Even though they do not contradict the existing error estimates, there are some convergence patterns that are worth commenting on:

- (1) The spatial convergence result for  $\sigma$  exhibits an even-odd behavior. Specifically, the rate is  $r$  for even order  $r$ , and it is  $r + 1$  when  $r$  is odd.
- (2) Extra orders of convergence (in space) for  $\nabla \cdot \mathbf{u}$  are observed for both the VPE and the VHE problems when the exact solution satisfies  $\nabla \cdot \mathbf{u} = 0$ . When the exact solutions are not divergence-free, there are no extra convergence orders for the divergence; however,  $\nabla \cdot \mathbf{u} = 0$  is the common situation for incompressible fluid flows, so the extra order is noteworthy.

Now that we have established the convergence results for the VHE with EBC, and compared them with the existing error estimates, we move on to the PPE reformulation. Note that, in this case, theoretical convergence results are not available. We numerically investigate the performance of the proposed schemes.

**3.4.2. Spatial Accuracy of the Time Dependent Stokes Problem.** We now conduct a spatial convergence study of the proposed method for the time-dependent Stokes PPE (3.1–3.2) discretized in space according to (3.5) and (3.8) and in time via the IMEX RK scheme (3.20). We consider the same domain,  $\Omega = [0, 1] \times [0, 1]$ , with periodic b.c. in the  $x$ -direction, EBC in the  $y$ -direction, and the same divergence-free velocity profile,  $\mathbf{u}(x, y, t)$ , as in §3.4.1. The pressure is taken to be

$$p = \cos(t) \cos(4\pi(x + y))(4y(1 - y))^4.$$

The forcing is fixed as  $\mathbf{f} = \mathbf{u}_t - \nu \Delta \mathbf{u} + \nabla p$ , and the initial conditions are chosen as  $\mathbf{u}_0 = \mathbf{u}(x, y, 0)$  (to match the manufactured solution). Both the manufactured solution and the forcing vanish at the boundary.

Following the same procedure as with the VHE above, we select the FE space  $(\sigma_h, \mathbf{u}_h, p_h) \in P_r \times RT_{r-1} \times P_r$ , with degrees  $r = 1, 2, 3, 4, 5$  on regular meshes. The time-stepping is done via IMEX(4,4,3), with fixed

Spatial approximation order $r = 1, (\sigma_h, \mathbf{u}_h) \in P_1 \times RT_0$								
$\Delta x$	$\mathbf{u}$	Rate	$\nabla \cdot \mathbf{u}$	Rate	$\sigma$	Rate	$\nabla \times \sigma$	Rate
2.50E-01	6.93E+00	—	9.97E+00	—	1.37E+02	—	2.76E+03	—
1.25E-01	3.26E+00	1.09	5.64E+00	0.82	3.19E+01	2.10	1.45E+03	0.92
6.25E-02	1.65E+00	0.98	1.04E+00	2.43	7.34E+00	2.12	7.24E+02	1.00
3.13E-02	8.24E-01	1.00	1.97E-01	2.41	1.77E+00	2.05	3.62E+02	1.00
1.56E-02	4.12E-01	1.00	4.57E-02	2.10	4.37E-01	2.01	1.81E+02	1.00
7.81E-03	2.06E-01	1.00	1.12E-02	2.03	1.09E-01	2.00	9.05E+01	1.00
Spatial approximation order $r = 2, (\sigma_h, \mathbf{u}_h) \in P_2 \times RT_1$								
$\Delta x$	$\mathbf{u}$	Rate	$\nabla \cdot \mathbf{u}$	Rate	$\sigma$	Rate	$\nabla \times \sigma$	Rate
2.50E-01	2.13E+00	—	8.82E+00	—	2.46E+01	—	1.25E+03	—
1.25E-01	7.89E-01	1.43	1.27E+00	2.80	7.50E+00	1.71	3.97E+02	1.66
6.25E-02	2.13E-01	1.89	2.31E-01	2.46	1.99E+00	1.91	1.04E+02	1.94
3.13E-02	5.45E-02	1.97	3.09E-02	2.90	5.01E-01	1.99	2.62E+01	1.98
1.56E-02	1.37E-02	1.99	3.92E-03	2.98	1.25E-01	2.00	6.57E+00	2.00
Spatial approximation order $r = 3, (\sigma_h, \mathbf{u}_h) \in P_3 \times RT_2$								
$\Delta x$	$\mathbf{u}$	Rate	$\nabla \cdot \mathbf{u}$	Rate	$\sigma$	Rate	$\nabla \times \sigma$	Rate
2.50E-01	1.32E+00	—	3.58E+00	—	1.88E+01	—	6.28E+02	—
1.25E-01	1.28E-01	3.37	2.27E-01	3.98	1.26E+00	3.90	7.40E+01	3.09
6.25E-02	1.56E-02	3.04	1.55E-02	3.87	7.96E-02	3.99	8.46E+00	3.13
3.13E-02	1.92E-03	3.02	9.67E-04	4.00	5.05E-03	3.98	1.05E+00	3.02
1.56E-02	2.40E-04	3.00	6.03E-05	4.00	3.17E-04	3.99	1.30E-01	3.00
Spatial approximation order $r = 4, (\sigma_h, \mathbf{u}_h) \in P_4 \times RT_3$								
$\Delta x$	$\mathbf{u}$	Rate	$\nabla \cdot \mathbf{u}$	Rate	$\sigma$	Rate	$\nabla \times \sigma$	Rate
2.50E-01	2.41E-01	—	1.68E+00	—	2.64E+00	—	1.52E+02	—
1.25E-01	1.74E-02	3.80	6.54E-02	4.68	1.70E-01	3.96	1.01E+01	3.91
6.25E-02	1.20E-03	3.85	1.04E-03	5.97	1.35E-02	3.66	6.98E-01	3.86
3.13E-02	7.73E-05	3.96	4.34E-05	4.58	8.98E-04	3.91	4.50E-02	3.95
1.56E-02	4.87E-06	3.99	2.27E-06	4.26	5.70E-05	3.98	2.84E-03	3.99
Spatial approximation order $r = 5, (\sigma_h, \mathbf{u}_h) \in P_5 \times RT_4$								
$\Delta x$	$\mathbf{u}$	Rate	$\nabla \cdot \mathbf{u}$	Rate	$\sigma$	Rate	$\nabla \times \sigma$	Rate
2.50E-01	8.56E-02	—	4.14E-01	—	1.27E+00	—	4.39E+01	—
1.25E-01	2.16E-03	5.31	7.33E-03	5.82	2.86E-02	5.48	1.47E+00	4.90
6.25E-02	6.31E-05	5.10	5.62E-05	7.03	4.64E-04	5.94	4.13E-02	5.15
3.13E-02	1.92E-06	5.04	8.70E-07	6.01	7.52E-06	5.95	1.27E-03	5.03
1.56E-02	5.97E-08	5.01	1.36E-08	6.00	1.19E-07	5.99	3.93E-05	5.01

TABLE 1. Observed spatial convergence rates in the  $L^2$  norm for the vector heat equation with electric boundary conditions (3.21). The spatial approximation orders are  $r = 1, 2, 3, 4, 5$ .

time step  $\Delta t = 10^{-5}$  and final time  $T = 10^{-3}$ . The stabilization parameter  $\lambda$  is set to be 10, following the suggestion in [55].

To avoid the approximation error introduced by iterative linear solvers, we use the sparse direct solver built into FEniCS. For the finest mesh resolution, and the 5th order spatial approximation, the sizes of the matrices for  $(\sigma, \mathbf{u})$  and  $p$  are  $656000 \times 656000$  and  $205121 \times 205121$ , respectively, which is close to the maximum that the direct solver could handle reliably.

Table 2 shows the spatial error convergence results for different degrees of the spatial approximation. The approximation errors are measured in the  $L^2$  norm. For quantities related to  $\mathbf{u}$  and  $\sigma$ , the rates of convergence have similar behaviors as for the VHE. Specifically: (i) the velocity  $\mathbf{u}$  is  $r$ -th order convergent for an  $r$ -th order spatial approximation, and (ii) the extra convergence orders for  $\nabla \cdot \mathbf{u}$  is carried over to the PPE reformulation. The convergence rate for the pressure  $p$  behaves similarly to  $\sigma$ , which appears in the right hand side of the weak formulation for the pressure in (3.8) and (3.9). However, non-clean pressure convergence rates are observed for approximation orders larger than 2.

It should be stressed that we numerically measure the convergence rate for the error in the velocity gradient  $\nabla \mathbf{u}$ , even though the FEM spaces do not guarantee that  $\nabla \mathbf{u}_h$  is in  $L^2$ . In particular, the numerical solution for the velocity is, generally, discontinuous (in the tangential direction) across Raviart-Thomas element edges. Here we measure the error in  $\nabla \mathbf{u}_h$  by ignoring the jumps across the edges, i.e. by only counting the error within each element. Note that it is of interest to measure the accuracy of velocity gradients as they relate to fluid stresses and forces at the boundary of objects. In addition, measuring the accuracy of fluid gradients will be a precursor to §4, in which  $\mathbf{u} \cdot \nabla \mathbf{u}$  will be included in the equations.

Spatial approximation order $r = 1, (\sigma_h, \mathbf{u}_h, p_h) \in P_1 \times RT_0 \times P_1$										
$\Delta x$	$\mathbf{u}$	Rate	$\nabla \cdot \mathbf{u}$	Rate	$\nabla \mathbf{u}$	Rate	$\sigma$	Rate	$p$	Rate
2.50E-01	6.93E+00	—	1.45E+01	—	1.37E+02	—	1.37E+02	—	3.39E+01	—
1.25E-01	3.26E+00	1.09	6.13E+00	1.25	1.37E+02	0.00	3.19E+01	2.10	3.38E+00	3.33
6.25E-02	1.65E+00	0.98	1.05E+00	2.54	1.37E+02	0.00	7.33E+00	2.12	4.41E-01	2.94
3.13E-02	8.24E-01	1.00	1.96E-01	2.42	1.37E+02	0.00	1.77E+00	2.05	1.08E-01	2.03
1.56E-02	4.12E-01	1.00	4.57E-02	2.10	1.37E+02	0.00	4.37E-01	2.01	2.71E-02	1.99
7.81E-03	2.06E-01	1.00	1.12E-02	2.02	1.37E+02	0.00	1.09E-01	2.00	6.78E-03	2.00
Spatial approximation order $r = 2, (\sigma_h, \mathbf{u}_h, p_h) \in P_2 \times RT_1 \times P_2$										
$\Delta x$	$\mathbf{u}$	Rate	$\nabla \cdot \mathbf{u}$	Rate	$\nabla \mathbf{u}$	Rate	$\sigma$	Rate	$p$	Rate
2.50E-01	2.09E+00	—	7.40E+00	—	9.33E+01	—	2.46E+01	—	1.80E+01	—
1.25E-01	7.88E-01	1.41	1.30E+00	2.51	6.25E+01	0.58	7.50E+00	1.71	7.64E-01	4.56
6.25E-02	2.13E-01	1.89	2.41E-01	2.43	3.27E+01	0.93	1.99E+00	1.91	6.18E-02	3.63
3.13E-02	5.45E-02	1.97	3.12E-02	2.95	1.66E+01	0.98	5.01E-01	1.99	1.05E-02	2.56
1.56E-02	1.37E-02	1.99	3.93E-03	2.99	8.33E+00	0.99	1.25E-01	2.00	2.45E-03	2.09
7.81E-03	3.43E-03	2.00	4.92E-04	3.00	4.17E+00	1.00	3.13E-02	2.00	6.08E-04	2.01
Spatial approximation order $r = 3, (\sigma_h, \mathbf{u}_h, p_h) \in P_3 \times RT_2 \times P_3$										
$\Delta x$	$\mathbf{u}$	Rate	$\nabla \cdot \mathbf{u}$	Rate	$\nabla \mathbf{u}$	Rate	$\sigma$	Rate	$p$	Rate
2.50E-01	1.33E+00	—	3.81E+00	—	7.09E+01	—	1.88E+01	—	4.33E+00	—
1.25E-01	1.28E-01	3.38	2.27E-01	4.07	1.67E+01	2.09	1.26E+00	3.90	1.46E-01	4.89
6.25E-02	1.56E-02	3.04	1.51E-02	3.92	4.24E+00	1.98	7.97E-02	3.99	6.91E-03	4.40
3.13E-02	1.92E-03	3.02	9.58E-04	3.97	1.06E+00	2.00	5.05E-03	3.98	2.96E-04	4.54
1.56E-02	2.40E-04	3.00	6.01E-05	4.00	2.66E-01	2.00	3.17E-04	4.00	1.47E-05	4.34
7.81E-03	2.99E-05	3.00	3.76E-06	4.00	6.65E-02	2.00	1.98E-05	4.00	9.81E-07	3.90
Spatial approximation order $r = 4, (\sigma_h, \mathbf{u}_h, p_h) \in P_4 \times RT_3 \times P_3$										
$\Delta x$	$\mathbf{u}$	Rate	$\nabla \cdot \mathbf{u}$	Rate	$\nabla \mathbf{u}$	Rate	$\sigma$	Rate	$p$	Rate
2.50E-01	2.41E-01	—	1.66E+00	—	1.94E+01	—	2.66E+00	—	1.17E+00	—
1.25E-01	1.74E-02	3.79	6.23E-02	4.74	3.03E+00	2.68	1.75E-01	3.92	4.83E-02	4.60
6.25E-02	1.20E-03	3.86	1.01E-03	5.95	4.04E-01	2.91	1.38E-02	3.67	3.00E-03	4.01
3.13E-02	7.73E-05	3.96	4.31E-05	4.55	5.14E-02	2.97	9.03E-04	3.93	1.12E-04	4.74
1.56E-02	4.87E-06	3.99	2.26E-06	4.25	6.46E-03	2.99	5.71E-05	3.98	4.62E-06	4.60
Spatial approximation order $r = 5, (\sigma_h, \mathbf{u}_h, p_h) \in P_5 \times RT_4 \times P_5$										
$\Delta x$	$\mathbf{u}$	Rate	$\nabla \cdot \mathbf{u}$	Rate	$\nabla \mathbf{u}$	Rate	$\sigma$	Rate	$p$	Rate
2.50E-01	8.61E-02	—	4.24E-01	—	6.56E+00	—	1.31E+00	—	4.88E-01	—
1.25E-01	2.17E-03	5.31	7.49E-03	5.82	4.80E-01	3.77	3.10E-02	5.40	1.36E-02	5.16
6.25E-02	6.33E-05	5.10	5.48E-05	7.10	3.14E-02	3.94	7.41E-04	5.39	5.86E-04	4.54
3.13E-02	1.93E-06	5.04	8.73E-07	5.97	1.98E-03	3.99	2.31E-05	5.00	2.19E-05	4.74
1.56E-02	5.97E-08	5.01	1.53E-08	5.83	1.24E-04	4.00	6.81E-07	5.09	6.70E-07	5.03

TABLE 2. Spatial error convergence in the  $L^2$  norm for the time dependent Stokes equation (3.1–3.2) in §3.4.2. The spatial approximations are  $(\sigma_h, \mathbf{u}_h, p_h) \in P_r \times RT_{r-1} \times P_r$ , with degrees  $r = 1, 2, 3, 4, 5$ . The calculations are done using  $\lambda = 10$  and the 3rd order IMEX(4,4,3), with a fixed small time step  $\Delta t = 10^{-5}$  and a fixed final time  $T = 10^{-3}$ .

3.4.3. *Temporal Accuracy of the Time Dependent Stokes Problem.* To check the temporal accuracy, we consider a manufactured solution on the same domain  $\Omega = [0, 1] \times [0, 1]$  with periodicity in the  $x$ -direction. The manufactured solution follows from the stream function

$$\psi(x, y, t) = \cos(200t) \sin^2(\pi x) \sin^2(\pi y),$$

so that the divergence-free condition is automatically satisfied by the velocity field  $\mathbf{u} = (u, v)^T = (\psi_y, -\psi_x)^T$ . The pressure is

$$p(x, y, t) = \cos(200t) \sin(2\pi x) \sin(\pi y).$$

Again, note that both the solution and the forcing vanish at the domain boundary. To test the temporal errors, we select a highly oscillatory in time manufactured solution. The high frequency oscillations in time ensure that the time discretization errors dominate the spatial discretization errors for the mesh resolution we use.

To perform the temporal error convergence study we solve the linear problem on a fixed mesh (mesh size  $\Delta x = 3.125 \times 10^{-2}$  and 4096 elements), a fixed FE discretization scheme (FE space with degree 4, that is  $(\sigma_h, \mathbf{u}_h, p_h) \in P_4 \times RT_3 \times P_4$ ), and a final time  $T = 0.5$ . Then we vary the time step:  $\Delta t = 2^{-k}$ ,  $k = 7, \dots, 13$ .

The temporal convergence results for the 3rd order IMEX(4,4,3) scheme are shown in Table 3. All quantities, except for the divergence  $\nabla \cdot \mathbf{u}$ , exhibit a 3rd order convergence in time in the  $L^2$  norm, while  $\nabla \cdot \mathbf{u}$  remains small for all  $\Delta t$ . The stagnation in the convergence for  $\nabla \mathbf{u}$ , at  $O(10^{-4})$ , is due to the spatial approximation error dominating the temporal error.

$\Delta t$	$\mathbf{u}$	Rate	$\nabla \cdot \mathbf{u}$	Rate	$\nabla \mathbf{u}$	Rate	$\sigma$	Rate	$p$	Rate
7.81E-03	7.725935E-02	—	6.531237E-08	—	5.932904E-01	—	5.932850E-01	—	9.039549E-02	—
3.91E-03	9.910506E-03	2.96	3.476197E-08	(0.91)	7.625508E-02	2.96	7.624960E-02	2.96	2.074725E-02	2.12
1.95E-03	1.269255E-03	2.97	3.004490E-08	(0.21)	9.693504E-03	2.98	9.685865E-03	2.98	3.396972E-03	2.61
9.77E-04	1.616344E-04	2.97	3.032122E-08	(-0.01)	1.233570E-03	2.97	1.207865E-03	3.00	4.883108E-04	2.80
4.88E-04	2.073504E-05	2.96	3.101061E-08	(-0.03)	2.734583E-04	(2.17)	1.495803E-04	3.01	6.545107E-05	2.90
2.44E-04	2.760336E-06	2.91	3.146726E-08	(-0.02)	2.270653E-04	(0.27)	1.894479E-05	2.98	8.380049E-06	2.97
1.22E-04	4.870641E-07	(2.50)	3.171521E-08	(-0.01)	2.259969E-04	(0.01)	2.585832E-06	(2.87)	1.032259E-06	3.02

TABLE 3. Temporal error convergence for (3.1–3.2) in the  $L^2$  norm for the 3rd order IMEX(4,4,3), on a fixed mesh, with the 4th order spatial discretization  $P_4 \times RT_3 \times P_4$ . The convergence rates in parentheses stagnate due to the spatial error dominating the temporal error.

3.4.4. *Convergence Results in Both Space and Time for the Time Dependent Stokes Equations.* Here we present the convergence results for a 3rd order scheme in both space and time applied to the time-dependent Stokes problem (3.1–3.2). We use the 3rd order spatial discretization  $(\sigma_h, \mathbf{u}_h, p_h) \in P_3 \times RT_2 \times P_3$  and the 3rd order time-stepping IMEX(4,4,3), with the time step scaled proportional to the mesh size — specifically  $\Delta t = 0.2\Delta x$ . A series of regular meshes with total number of elements 64, 256, 1024, 4096, 16384 and 65536 are used. On the finest mesh, the sizes of the linear systems are 983808 for  $(\mathbf{u}, \sigma)$  and 295297 for  $p$ . The manufactured solution is chosen to be

$$\mathbf{u} = \psi_y, \quad v = -\psi_x, \quad p = \pi \cos(t) \cos(\pi x) \sin(\pi y) (4x(1-x))^4 (4y(1-y))^4,$$

where  $\psi(x, y, t) = \cos(t) \sin^2(\pi x) \sin^2(\pi y) (4x(1-x))^4 (4y(1-y))^4$ , on the unit square domain  $\Omega = [0, 1]^2$ . The EBC are prescribed at all boundaries. *This test differs from the previous tests where periodic b.c. in  $x$  were used.* Again, the exact solution is constructed so that the velocity and the forcing vanish at the boundary.

Table 4 shows the error convergence results in the  $L^2$  norm (top) and in the  $L^\infty$  norm (bottom). Clean convergence are observed for  $\mathbf{u}$ ,  $\nabla \mathbf{u}$  and  $\nabla \cdot \mathbf{u}$ , with rates 3, 2 and 4 respectively. Non-clean convergence rates occur for  $\sigma$ ,  $\nabla \times \sigma$ ,  $p$  and  $\nabla p$ . However, they appear to be close to 3.

Error convergence in the $L^2$ norm														
$\Delta x$	$\mathbf{u}$	Rate	$\nabla \cdot \mathbf{u}$	Rate	$\nabla \mathbf{u}$	Rate	$\sigma$	Rate	$\nabla \times \sigma$	Rate	$p$	Rate	$\nabla p$	Rate
2.50E-01	4.27E-02	—	9.84E-02	—	2.91E+00	—	3.22E-01	—	1.40E+01	—	1.99E-01	—	5.37E+00	—
1.25E-01	8.12E-03	2.39	8.25E-03	3.57	1.03E+00	1.51	2.48E-02	3.70	2.08E+00	2.75	2.76E-03	6.17	2.11E-01	4.67
6.25E-02	1.04E-03	2.96	5.87E-04	3.81	2.62E-01	1.97	2.81E-03	3.14	2.76E-01	2.91	3.53E-04	2.96	3.09E-02	2.77
3.13E-02	1.33E-04	2.97	3.76E-05	3.96	6.57E-02	2.00	4.57E-04	2.62	3.56E-02	2.96	9.88E-05	1.84	5.14E-03	2.59
1.56E-02	1.69E-05	2.97	2.37E-06	3.99	1.64E-02	2.00	7.66E-05	2.58	4.56E-03	2.96	2.33E-05	2.08	6.73E-04	2.93
7.81E-03	2.14E-06	2.99	1.49E-07	3.99	4.11E-03	2.00	1.14E-05	2.74	5.83E-04	2.97	2.91E-06	3.00	7.65E-05	3.13
Error convergence in the $L^\infty$ norm														
$\Delta x$	$\mathbf{u}$	Rate	$\nabla \cdot \mathbf{u}$	Rate	$\nabla \mathbf{u}$	Rate	$\sigma$	Rate	$\nabla \times \sigma$	Rate	$p$	Rate	$\nabla p$	Rate
2.50E-01	2.42E-01	—	3.10E-01	—	1.30E+01	—	2.32E+00	—	1.05E+02	—	1.23E+00	—	2.87E+01	—
1.25E-01	1.12E-01	1.12	4.46E-02	2.80	7.80E+00	0.74	1.54E-01	3.91	2.26E+01	2.21	3.44E-02	5.16	1.45E+00	4.31
6.25E-02	1.77E-02	2.65	3.17E-03	3.81	2.12E+00	1.88	1.92E-02	3.01	2.52E+00	3.16	3.99E-03	3.11	4.28E-01	1.76
3.13E-02	2.34E-03	2.92	2.06E-04	3.95	5.36E-01	1.98	2.68E-03	2.84	3.66E-01	2.79	7.06E-04	2.50	9.46E-02	2.18
1.56E-02	2.97E-04	2.98	1.29E-05	4.00	1.34E-01	2.00	4.05E-04	2.73	5.34E-02	2.78	1.26E-04	2.48	1.42E-02	2.74
7.81E-03	3.73E-05	2.99	8.00E-07	4.01	3.35E-02	2.00	6.02E-05	2.75	5.91E-03	3.18	1.52E-05	3.05	2.29E-03	2.63

TABLE 4. Error convergence for the linear problem without the advection term (3.1–3.2) in the  $L^2$  norm (top) and the  $L^\infty$  norm (bottom). The problem is solved with the 3rd order IMEX RK scheme (IMEX(4,4,3)), the 3rd order spatial discretization  $P_3 \times RT_2 \times P_3$ , and  $\lambda = 30$ .

Figure 2 shows the pressure error and the divergence, as functions of  $(x, y)$ , at the final time  $T = 3$ . No numerical boundary layers are observed in the pressure error. The divergence at the final time is small at the boundary, but not exactly zero. This is due to the fact that the divergence boundary condition is only enforced weakly in the mixed formulation (appears as a natural boundary condition). The dynamics of the PPE reformulation ( $\nabla \cdot \mathbf{u}$  satisfies a heat equation) keeps the divergence small across the domain.

In the PPE reformulation, there is no inf-sup condition for the velocity and the pressure. This is in contrast to the conventional FEM formulation for the Navier-Stokes equations, in which the finite element

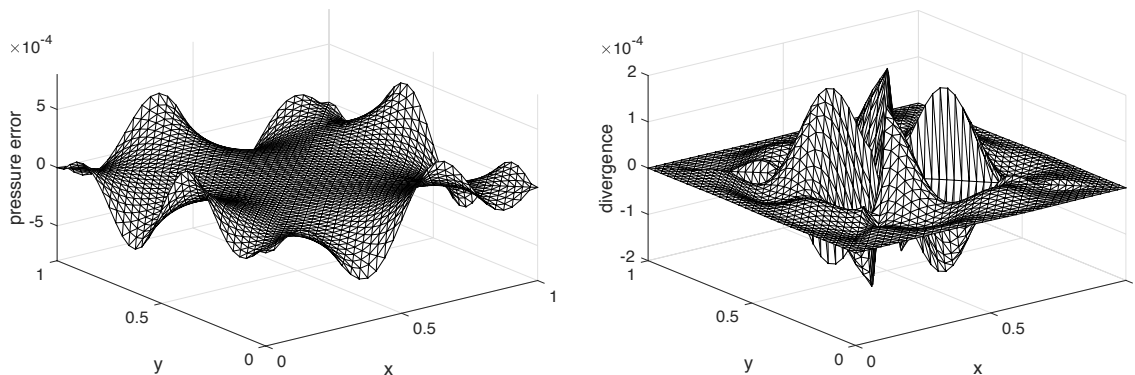


FIGURE 2. Errors in the pressure (left) and the divergence (right) for the time dependent Stokes equations in §3.4.4, as functions of  $(x, y)$ , at the final time  $T = 3$ . The plot is for the 3rd order IMEX(4,4,3) with a 3rd order ( $r = 3$ ) spatial discretization on a regular mesh with 4096 elements.

spaces for the velocity and the pressure need to satisfy the discrete version of the inf-sup condition to ensure stability. Hence the orders of the spatial approximations for  $(\sigma_h, \mathbf{u}_h) \in P_r \times RT_{r-1}$  and the pressure  $p_h \in P_r$  could be selected independently. However, we observed in the numerical experiments that: *if the pressure approximation is one order less than the velocity approximation, the error convergence for the divergence decreases by one compared to the equal-order case.* Furthermore: *increasing the order of approximation for the pressure does not improve the convergence rates compared to the equal-order case.*

**Remark 3.3.** (*Degradation of convergence rates*) Some of the convergence rates in Table 4 do not exhibit a clear integer rate. A possible explanation for the reduction in convergence rate is provided in [3] (Theorems 5.1–5.2), where it is shown that a mixed finite element approximation for the Stokes equations exhibits a degraded convergence rate.

3.4.5. *Influence of the parameter  $\lambda$ .* The role of the parameter  $\lambda$  in the PPE reformulation (2.5–2.6) is to exponentially enforce the normal velocity condition at the boundary, as highlighted by the ODE (2.8). If  $\lambda = 0$ , the exact solution to the ODE (2.8) still satisfies  $\mathbf{n} \cdot \mathbf{u} = \mathbf{n} \cdot \mathbf{g}$  (when  $\phi = 0$ ), however the numerical scheme exhibits a steady growth of the error, as described in [55]. Our numerical experiments show that when  $\lambda$  is set to 0, there are degradations in the convergence rates for  $\mathbf{u}$ ,  $\sigma$  and the pressure  $p$ , even though a 3rd order scheme is used. Increasing  $\lambda$  controls the error in the velocity and hence improves the accuracy of the overall scheme (see Table 5).

It is worth mentioning that the convergence rate of  $\nabla \cdot \mathbf{u}$ , even the error in  $\nabla \cdot \mathbf{u}$ , seems to be unaffected by the choice of  $\lambda$ . This is due to the fact that the enforcement of the divergence condition derives from the fact that the divergence (implicitly) satisfies the heat equation (2.7), with homogeneous boundary condition. Hence it is independent of the parameter  $\lambda$ . When  $\lambda = 0$  the normal velocity condition is enforced poorly, thus there is (numerical) flow through the boundary. But the divergence is small, hence the total flow through the boundary should be small, with inflows compensated by outflows.

#### 4. TREATMENT OF THE NONLINEAR ADVECTION TERM

Next, in §4.1, we explore avenues for discretizing the nonlinear advection term in the mixed finite element framework introduced in §3. Although the approach we present is ad hoc, the numerical results in §4.2 indicate that the full scheme is convergent, with a little degradation in the rates of convergence relative to the linearized equations. Benchmark test results for the lid-driven cavity and the backward-facing step flow are presented in §4.3, which show good agreement with the reference data.

**4.1. Discretization of the nonlinear advection term.** In §3, we introduced a mixed finite element spatial discretization as a way to handle the electric boundary conditions (EBC) for the vector heat equation and time-dependent Stokes equation. While the mixed finite elements resolve several difficulties for the

Error convergence in the $L^2$ norm with $\lambda = 0$										
$\Delta x$	$\mathbf{u}$	Rate	$\nabla \cdot \mathbf{u}$	Rate	$\nabla \mathbf{u}$	Rate	$\sigma$	Rate	$p$	Rate
2.50E-01	5.61E-02	—	9.60E-02	—	2.95E+00	—	5.06E-01	—	4.39E-01	—
1.25E-01	3.47E-02	0.69	8.24E-03	3.54	1.06E+00	1.48	2.51E-01	1.01	1.88E-01	1.23
6.25E-02	1.81E-02	0.94	5.86E-04	3.81	2.97E-01	1.84	1.35E-01	0.89	1.07E-01	0.81
3.13E-02	5.65E-03	1.68	3.76E-05	3.96	7.99E-02	1.89	4.51E-02	1.59	3.86E-02	1.47
1.56E-02	9.61E-04	2.55	2.37E-06	3.99	1.89E-02	2.08	9.26E-03	2.28	8.58E-03	2.17
Error convergence in the $L^2$ norm with $\lambda = 30$										
$\Delta x$	$\mathbf{u}$	Rate	$\nabla \cdot \mathbf{u}$	Rate	$\nabla \mathbf{u}$	Rate	$\sigma$	Rate	$p$	Rate
2.50E-01	4.27E-02	—	9.84E-02	—	2.91E+00	—	3.22E-01	—	1.99E-01	—
1.25E-01	8.12E-03	2.39	8.25E-03	3.57	1.03E+00	1.51	2.48E-02	3.70	2.76E-03	6.17
6.25E-02	1.04E-03	2.96	5.87E-04	3.81	2.62E-01	1.97	2.81E-03	3.14	3.53E-04	2.96
3.13E-02	1.33E-04	2.97	3.76E-05	3.96	6.57E-02	2.00	4.57E-04	2.62	9.88E-05	1.84
1.56E-02	1.69E-05	2.97	2.37E-06	3.99	1.64E-02	2.00	7.66E-05	2.58	2.33E-05	2.08
7.81E-03	2.14E-06	2.99	1.49E-07	3.99	4.11E-03	2.00	1.14E-05	2.74	2.91E-06	3.00

TABLE 5. Error convergence in the  $L^2$  norm for the linear problem (3.1–3.2) with  $\lambda = 0$  (top) and  $\lambda = 30$  (bottom). The problem is solved with the 3rd order approximation  $P_3 \times RT_2 \times P_3$  and the 3rd order IMEX(4,4,3), using the same manufactured solution in §3.4.4.

EBC, they come with a caveat:  $RT$  elements approximating  $\mathbf{u}$  are only guaranteed to be continuous across interior edges in the normal direction but can jump in the tangential direction. Therefore, representations of the discrete solution using  $RT$  elements are only weakly differentiable along the normal direction across edges. This creates a problem then for handling nonlinear advection terms  $\mathbf{N}(\mathbf{u}) = (\mathbf{u} \cdot \nabla)\mathbf{u}$ , and in fact, even linear advection terms  $(\mathbf{a} \cdot \nabla)\mathbf{u}$ . Specifically, in 2D,  $RT$  elements approximate a function  $\mathbf{u}$   $\mathbf{v} = (v_1, v_2)^T \in H(\text{div}; \Omega)$ , i.e.  $v_1, v_2, \nabla \cdot \mathbf{v} \in L^2(\Omega)$ . In general, each component of  $\nabla \mathbf{v}$  is not guaranteed to be in  $L^2$ , therefore for any  $\mathbf{u}, \mathbf{v} \in H(\text{div}; \Omega)$  the inner product

$$(4.1) \quad \langle (\mathbf{a} \cdot \nabla)\mathbf{u}, \mathbf{v} \rangle = \int_{\Omega} (\mathbf{a} \cdot \nabla)\mathbf{u} \cdot \mathbf{v} \, dV$$

is not properly defined.

However, when the numerical approximation  $\mathbf{u}_h$ , which is represented by  $RT$  elements, is restricted to each triangular element  $\mathcal{T}$ , the components of  $\mathbf{u}_h|_{\mathcal{T}}$  are polynomials and thus differentiable *within*  $\mathcal{T}$ . Hence, we consider the integral (4.1) in an element-wise sense. Let  $\Omega_h$  be a triangulation of the domain  $\Omega \subset \mathbb{R}^N$ . Then the integral involving the nonlinear advection term  $\mathbf{N}(\mathbf{u})$  can then be approximated by

$$(4.2) \quad \langle \mathbf{N}(\mathbf{u}_h), \mathbf{v}_h \rangle_{\mathcal{T}} = \sum_{\mathcal{T} \in \Omega_h} \int_{\mathcal{T}} \mathbf{N}(\mathbf{u}_h) \cdot \mathbf{v}_h \, dV, \quad \forall \mathbf{v}_h \in RT_r(\Omega_h),$$

where  $RT_r(\Omega_h)$  is the Raviart-Thomas finite element space that approximates  $H(\text{div}; \Omega_h)$ , with  $\nabla \mathbf{u}_h$  defined in each element  $\mathcal{T} \in \Omega_h$ .

**4.2. Numerical Results on Manufactured Solutions.** In this subsection, we present convergence results for the full scheme: PPE reformulation with the nonlinear advection term treated as described in the previous subsection. To test the treatment of the advection term without the complications from the PPE reformulation, we first study the spatial convergence of the mixed formulation applied to the vector advection-diffusion equation with electric boundary conditions. We then present the convergence results for the full problem with the nonlinear term.

**4.2.1. Vector Nonlinear Advection-diffusion Equation with EBC.** To study the performance of the proposed treatment (4.2) of the advection term, we consider the same semi-periodic domain and manufactured solution as in §3.4.1, but for the vector-valued nonlinear advection-diffusion equation:

$$(4.3) \quad \mathbf{u}_t + (\mathbf{u} \cdot \nabla)\mathbf{u} = \Delta \mathbf{u} + \mathbf{f} \quad \text{for } (x, y) \in (0, 1)^2,$$

$$(4.4) \quad \mathbf{n} \times \mathbf{u} = 0, \quad \nabla \cdot \mathbf{u} = 0 \quad \text{for } (x, y) \in [0, 1) \times \{0, 1\},$$

$$(4.5) \quad \mathbf{u}(0, y) = \mathbf{u}(1, y) \quad \text{for } 0 < y < 1.$$

In the presence of the nonlinear advection term, systematic degradations in the spatial convergence order are observed (see Table 6). Specifically, non-convergent result is observed for  $r = 1$ . For  $r = 2, 4$ , the

convergence rates are  $r$ ,  $r$ ,  $r - 1$ ,  $r$  and  $r - 1$  for  $\mathbf{u}$ ,  $\nabla \cdot \mathbf{u}$ ,  $\nabla \mathbf{u}$ ,  $\sigma$  and  $\nabla \times \sigma$ , respectively (in both the  $L^2$  and  $L^\infty$  norms). The convergence rates are less clean when  $r$  is odd, but follow a similar pattern as in the even order case. These results indicate that degradation in the convergence order for the full PPE reformulation (2.5–2.6) should be expected.

Spatial approximation order $r = 1$ , $(\sigma_h, \mathbf{u}_h, p_h) \in P_1 \times RT_0 \times P_1$										
$\Delta x$	$\mathbf{u}$	Rate	$\nabla \cdot \mathbf{u}$	Rate	$\nabla \mathbf{u}$	Rate	$\sigma$	Rate	$\nabla \times \sigma$	Rate
2.50E-01	6.93E+00	—	1.00E+01	—	1.37E+02	—	1.37E+02	—	2.76E+03	—
1.25E-01	3.28E+00	1.08	5.92E+00	0.76	1.37E+02	0.00	3.19E+01	2.10	1.45E+03	0.92
6.25E-02	1.67E+00	0.97	2.36E+00	1.33	1.37E+02	0.00	7.60E+00	2.07	7.25E+02	1.00
3.13E-02	8.75E-01	0.94	2.24E+00	0.07	1.37E+02	0.00	2.82E+00	1.43	3.65E+02	0.99
1.56E-02	5.07E-01	0.79	2.27E+00	-0.02	1.37E+02	-0.00	2.30E+00	0.30	1.87E+02	0.97
7.81E-03	3.60E-01	0.49	2.28E+00	-0.01	1.37E+02	-0.00	2.27E+00	0.02	1.01E+02	0.88
Spatial approximation order $r = 2$ , $(\sigma_h, \mathbf{u}_h, p_h) \in P_2 \times RT_1 \times P_2$										
$\Delta x$	$\mathbf{u}$	Rate	$\nabla \cdot \mathbf{u}$	Rate	$\nabla \mathbf{u}$	Rate	$\sigma$	Rate	$\nabla \times \sigma$	Rate
2.50E-01	2.13E+00	—	9.11E+00	—	9.33E+01	—	2.47E+01	—	1.25E+03	—
1.25E-01	7.92E-01	1.43	1.77E+00	2.37	6.26E+01	0.58	7.62E+00	1.70	4.03E+02	1.64
6.25E-02	2.14E-01	1.89	4.20E-01	2.07	3.28E+01	0.93	2.07E+00	1.88	1.17E+02	1.79
3.13E-02	5.48E-02	1.97	8.91E-02	2.24	1.66E+01	0.98	5.23E-01	1.98	3.92E+01	1.57
1.56E-02	1.38E-02	1.99	2.10E-02	2.08	8.33E+00	0.99	1.31E-01	2.00	1.63E+01	1.27
7.81E-03	3.45E-03	2.00	5.18E-03	2.02	4.17E+00	1.00	3.27E-02	2.00	7.65E+00	1.09
Spatial approximation order $r = 3$ , $(\sigma_h, \mathbf{u}_h, p_h) \in P_3 \times RT_2 \times P_3$										
$\Delta x$	$\mathbf{u}$	Rate	$\nabla \cdot \mathbf{u}$	Rate	$\nabla \mathbf{u}$	Rate	$\sigma$	Rate	$\nabla \times \sigma$	Rate
2.50E-01	1.33E+00	—	3.90E+00	—	7.10E+01	—	1.90E+01	—	6.41E+02	—
1.25E-01	1.28E-01	3.37	3.47E-01	3.49	1.67E+01	2.09	1.32E+00	3.85	8.12E+01	2.98
6.25E-02	1.58E-02	3.02	4.27E-02	3.02	4.24E+00	1.98	1.00E-01	3.72	1.16E+01	2.80
3.13E-02	2.03E-03	2.96	6.82E-03	2.65	1.06E+00	2.00	1.13E-02	3.16	2.25E+00	2.37
1.56E-02	2.90E-04	2.81	1.43E-03	2.25	2.66E-01	2.00	2.06E-03	2.45	5.15E-01	2.13
Spatial approximation order $r = 4$ , $(\sigma_h, \mathbf{u}_h, p_h) \in P_4 \times RT_3 \times P_4$										
$\Delta x$	$\mathbf{u}$	Rate	$\nabla \cdot \mathbf{u}$	Rate	$\nabla \mathbf{u}$	Rate	$\sigma$	Rate	$\nabla \times \sigma$	Rate
2.50E-01	2.42E-01	—	1.72E+00	—	1.94E+01	—	2.71E+00	—	1.57E+02	—
1.25E-01	1.74E-02	3.80	7.45E-02	4.53	3.03E+00	2.68	1.80E-01	3.91	1.16E+01	3.76
6.25E-02	1.20E-03	3.86	2.53E-03	4.88	4.04E-01	2.91	1.40E-02	3.68	1.09E+00	3.41
3.13E-02	7.74E-05	3.96	1.33E-04	4.25	5.14E-02	2.97	9.28E-04	3.92	1.16E-01	3.22
1.56E-02	4.88E-06	3.99	7.79E-06	4.09	6.46E-03	2.99	5.89E-05	3.98	1.38E-02	3.07
Spatial approximation order $r = 5$ , $(\sigma_h, \mathbf{u}_h, p_h) \in P_5 \times RT_4 \times P_4$										
$\Delta x$	$\mathbf{u}$	Rate	$\nabla \cdot \mathbf{u}$	Rate	$\nabla \mathbf{u}$	Rate	$\sigma$	Rate	$\nabla \times \sigma$	Rate
2.50E-01	8.59E-02	—	4.32E-01	—	6.56E+00	—	1.28E+00	—	4.61E+01	—
1.25E-01	2.17E-03	5.31	8.36E-03	5.69	4.81E-01	3.77	2.93E-02	5.45	1.82E+00	4.66
6.25E-02	6.37E-05	5.09	1.74E-04	5.59	3.14E-02	3.94	5.27E-04	5.80	7.55E-02	4.59
3.13E-02	1.99E-06	5.00	7.18E-06	4.60	1.98E-03	3.99	1.28E-05	5.36	4.10E-03	4.20
1.56E-02	6.80E-08	4.87	3.68E-07	4.29	1.24E-04	4.00	5.41E-07	4.57	2.46E-04	4.06

TABLE 6. Observed spatial convergence rates in the  $L^2$  norm for the vector nonlinear advection-diffusion equation with electric boundary conditions (4.3–4.5). The spatial approximation orders are  $r = 1, 2, 3, 4, 5$ .

4.2.2. *The PPE Reformulation (2.5–2.6) (including the Nonlinear Advection Term)*. Consider the same manufactured solution, defined on the unit square  $\Omega = [0, 1]^2$ , as in §3.4.4. However, since here we solve the full problem (2.5–2.6), the forcing function is given by  $\mathbf{f} = \mathbf{u}_t + (\mathbf{u} \cdot \nabla)\mathbf{u} - \nu \Delta \mathbf{u} + \nabla p$ . We then use: the 3rd order spatial discretization  $(\sigma_h, \mathbf{u}_h, p_h) \in P_3 \times RT_2 \times P_3$ , the 3rd order IMEX(4,4,3) with time step  $\Delta t = 0.2\Delta x$ , the final time  $T = 3$ , and  $\lambda = 30$  (the same as in the previous test cases).

The error convergence are shown in Table 7 in the  $L^2$  norm (top) and in the  $L^\infty$  norm (bottom). Convergent results are observed for all quantities but with slightly degraded convergence rates in comparison to the linear case in Table 4. In particular, the convergence rate for  $\nabla \cdot \mathbf{u}$  is a little bigger than 3 as opposed to 4 in the linear case, and  $\nabla \times \sigma$ ,  $p$  and  $\nabla p$  show a 2nd order convergence.

4.3. **Numerical Results on Benchmark Tests.** In this subsection, we demonstrate the performance of the proposed method for solving two benchmark problems: lid-driven cavity in §4.3.1, and flow over a backward-facing step in §4.3.2. The results show good agreement with reference data.

Error convergence in $L^2$ norm														
$\Delta x$	$\mathbf{u}$		$\nabla \cdot \mathbf{u}$		$\nabla \mathbf{u}$		$\sigma$		$\nabla \times \sigma$		$p$	$\nabla p$		
2.50E-01	4.28E-02	—	1.02E-01	—	2.92E+00	—	3.37E-01	—	1.47E+01	—	2.60E-01	—	5.70E+00	—
1.25E-01	8.14E-03	2.40	9.39E-03	3.45	1.03E+00	1.51	3.52E-02	3.26	2.97E+00	2.30	5.33E-02	2.28	9.49E-01	2.59
6.25E-02	1.05E-03	2.96	7.22E-04	3.70	2.62E-01	1.97	4.74E-03	2.89	5.93E-01	2.33	1.45E-02	1.87	2.42E-01	1.97
3.13E-02	1.36E-04	2.95	5.89E-05	3.62	6.57E-02	2.00	8.15E-04	2.54	1.37E-01	2.12	3.69E-03	1.98	6.11E-02	1.99
1.56E-02	1.84E-05	2.88	5.91E-06	3.32	1.64E-02	2.00	1.64E-04	2.31	3.34E-02	2.03	9.18E-04	2.01	1.52E-02	2.01
7.81E-03	2.70E-06	2.77	6.84E-07	3.11	5.64E-03	1.54	3.68E-05	2.16	8.30E-03	2.01	2.28E-04	2.01	3.82E-03	1.99
Error convergence in $L^\infty$ norm														
$\Delta x$	$\mathbf{u}$		$\nabla \cdot \mathbf{u}$		$\nabla \mathbf{u}$		$\sigma$		$\nabla \times \sigma$		$p$	$\nabla p$		
2.50E-01	2.37E-01	—	3.20E-01	—	1.30E+01	—	2.32E+00	—	1.05E+02	—	1.24E+00	—	2.87E+01	—
1.25E-01	1.12E-01	1.09	7.30E-02	2.13	7.80E+00	0.74	2.31E-01	3.33	2.30E+01	2.19	3.51E-01	1.83	5.27E+00	2.45
6.25E-02	1.77E-02	2.65	5.69E-03	3.68	2.12E+00	1.88	3.58E-02	2.69	3.97E+00	2.54	9.41E-02	1.90	1.89E+00	1.48
3.13E-02	2.34E-03	2.92	3.56E-04	4.00	5.36E-01	1.98	4.99E-03	2.85	9.46E-01	2.07	2.34E-02	2.01	5.60E-01	1.76
1.56E-02	2.97E-04	2.98	2.98E-05	3.58	1.34E-01	2.00	7.17E-04	2.80	2.38E-01	1.99	5.78E-03	2.02	1.47E-01	1.93
7.81E-03	3.73E-05	2.99	3.15E-06	3.24	3.35E-02	2.00	1.46E-04	2.29	6.02E-02	1.98	1.43E-03	2.01	3.73E-02	1.97

TABLE 7. Error convergence for the full Navier-Stokes problem (including the nonlinear advection term) in the  $L^2$  norm (top) and the  $L^\infty$  norm (bottom). The problem is solved with the 3rd order time-stepping IMEX(4,4,3), the 3rd order spatial discretization  $P_3 \times RT_2 \times P_3$ , the final time  $T = 3$ , and  $\lambda = 30$ .

4.3.1. *Lid-driven Cavity.* For the lid-driven cavity, we compute the flow in the unit square domain  $[0, 1]^2$ , with  $\lambda = 10$ , using the 3rd order spatial approximation  $P_3 \times RT_2 \times P_3$  and 3rd order IMEX RK time-stepping (time step  $\Delta t = 0.8\Delta x$ ), on a regular triangular mesh with 16384 elements and a mesh size  $\Delta x = 1.5625 \times 10^{-2}$ . The velocity field is advanced forward in time until it reaches steady state, for Reynolds numbers 100, 400 and 1000. The flow starts at rest, with boundary conditions  $\mathbf{g} = (1, 0)^T$  at the top wall and no-slip elsewhere.

The results for  $Re = 100$ , 400 and 1000 are shown in Figures 3–5. The streamlines for the steady state flow are shown in the left panel of each figure.<sup>1</sup> The velocity profiles along the centerlines of the cavity (i.e.  $u(0.5, y)$  and  $v(x, 0.5)$ ) are plotted in the right panel, together with the reference data from [21]. Note that some streamlines in the plots end at the domain boundary, without forming closed curves. This is due to the following facts: (i) the numerical solution is not exactly divergence-free, (ii) the normal velocity condition at the boundary is not enforced strongly (in the Dirichlet sense) but rather through the ODE (2.8), which results in a small (as small as the resolution) flow through the boundary. The flow through the boundary is more pronounced at the top corners, where discontinuities in the velocity occurs. Increasing  $\lambda$  makes the enforcing of the normal velocity condition stronger, and reduces the flow through the boundary. However, making  $\lambda$  too big would impose an undesirable time step restriction,  $\Delta t < O(\frac{1}{\lambda})$ , through the relaxation term in (2.8).

4.3.2. *Backward-facing Step.* In this test case, we compute the benchmark problem of flow over a backward-facing step for  $Re = 100$  and  $Re = 200$ . Again, we use the 3rd order spatial discretization  $P_3 \times RT_2 \times P_3$ , a 3rd order IMEX RK scheme and  $\lambda = 10$ . The computation uses a non-uniform triangular mesh with extra mesh refinement near the reentrant corner and the region behind the step. The minimum mesh size is  $\Delta x = 1.7028 \times 10^{-2}$  and the time step is set to  $\Delta t = 0.02\Delta x$ . In this case the domain of computation is

$$\Omega = [0, L] \times [-0.5, 0.5] \setminus [0, 0.5] \times [-0.5, 0],$$

where  $L$  is the channel length, set to  $L = 8$ . No-slip boundary conditions are imposed everywhere, except for the inflow and outflow boundaries at  $x = 0$  and  $x = L$ . The inflow and outflow boundary conditions are

$$\mathbf{g}_{\text{inflow}} = f(t) (12y(1 - 2y), 0)^T,$$

$$\mathbf{g}_{\text{outflow}} = f(t) \left( -3y^2 + \frac{3}{4}, 0 \right)^T,$$

where  $f(t) = 1 - e^{-6t^2}$ , so that the flow is initially at rest and the inflow and outflow increase gradually with time. The mean inflow velocity  $U$  reaches 1 for large enough  $t$ . We use the channel height  $H = 1$  as the characteristic length, which gives a Reynolds number  $Re = HU/\nu = 1/\nu$ .

<sup>1</sup> The streamlines at the final time,  $T$ , are computed by numerically solving the ODE  $\frac{d\mathbf{x}}{ds} = \mathbf{u}(\mathbf{x}, T)$  with an explicit 4th order Runge-Kutta (RK4) scheme).

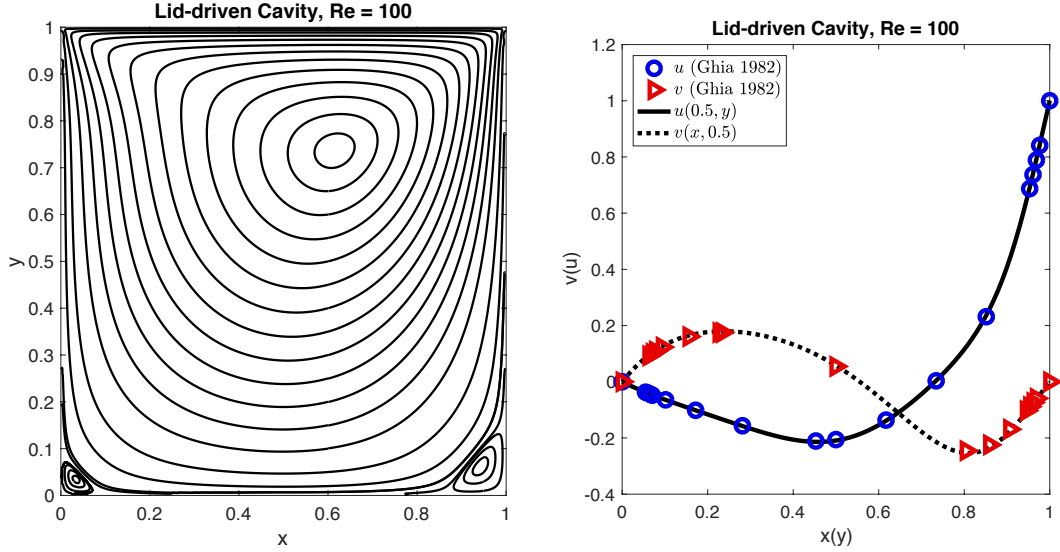


FIGURE 3. Lid-driven cavity flow with  $Re = 100$ . Left: Streamlines at steady state. Right: Velocity profiles along the centerlines (solid line:  $u(0.5, y)$ , and dashed line:  $v(x, 0.5)$ ) compared with the reference data (blue circles and red triangles) in [21].

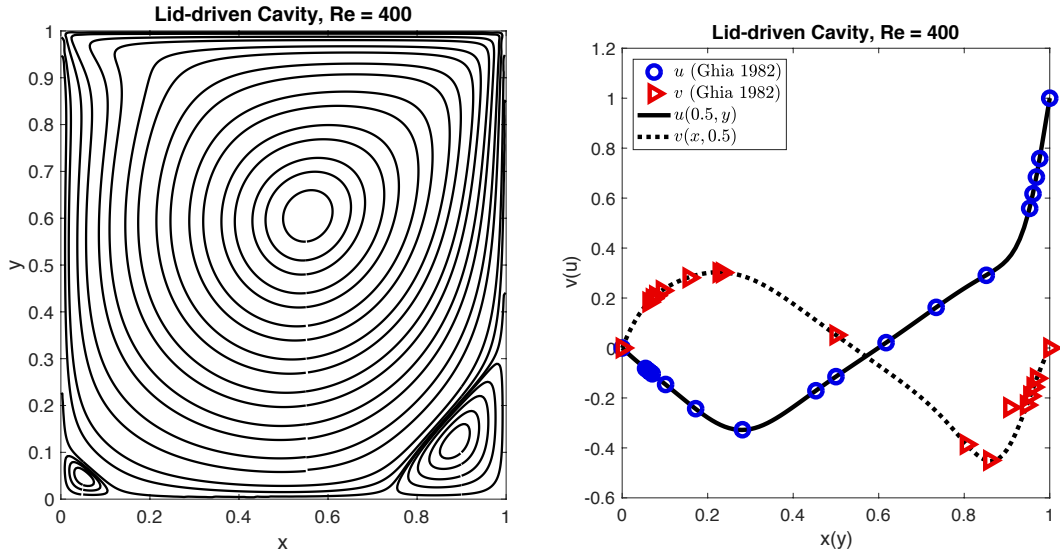


FIGURE 4. Lid-driven cavity flow with  $Re = 400$ . Left: Streamlines at steady state. Right: Velocity profiles along the centerlines (solid line:  $u(0.5, y)$ , and dashed line:  $v(x, 0.5)$ ) compared with the reference data (blue circles and red triangles) in [21].

For  $Re = 100$  and  $200$ , the only recirculating flow forms behind the step. More regions of recirculating flow appear down the channel as the Reynolds number increases. The streamlines shown in Figure 6 were computed using the same procedure described in §4.3.1.

To compare our results with the reference data in [18] we use the position of the reattachment point, where the line separating the recirculating flow behind the step and the main flow in the channel meets the channel wall, i.e. the domain boundary. For this purpose introduce the nondimensional ratio  $L_1/S$ , where  $L_1$  is the distance between the foot of the step and the reattachment point, and  $S = 0.5$  is the step height. For  $Re = 100$ , the ratio  $L_1/S = 2.96$  in our computation compares well with the reference data ratio: 2.922. For  $Re = 200$ , our computation yields a ratio  $L_1/S = 4.86$ , while the reference value is 4.982. Our results show a rather good agreement with the reference values.

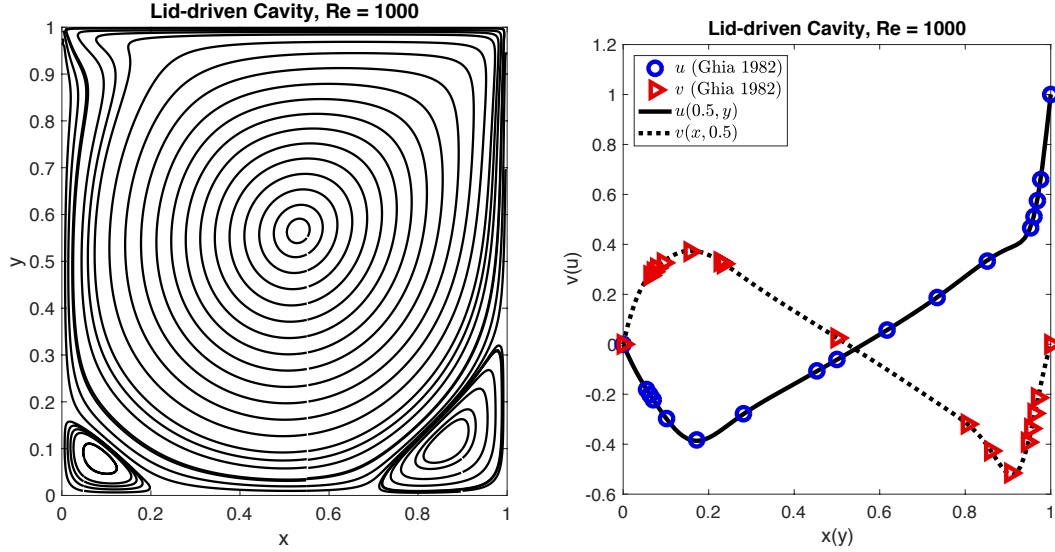


FIGURE 5. Lid-driven cavity flow with  $Re = 1000$ . Left: Streamlines at steady state. Right: Velocity profiles along the centerlines (solid line:  $u(0.5, y)$ , and dashed line:  $v(x, 0.5)$ ) compared with the reference data (blue circles and red triangles) in [21].

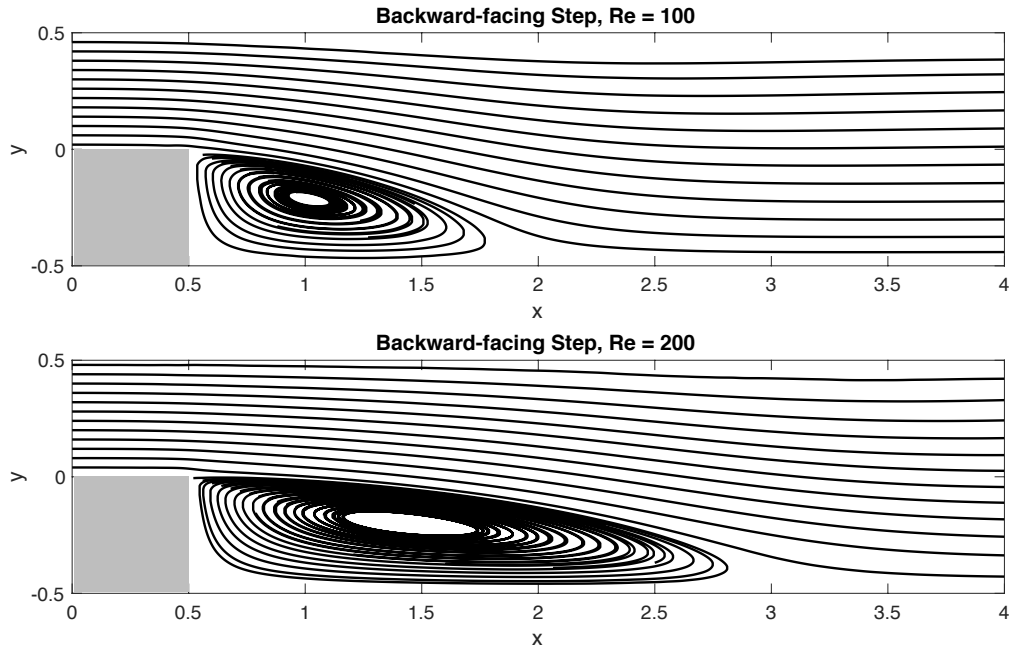


FIGURE 6. Streamlines for the computation of a flow over a backward-facing step, at steady state, for  $Re = 100$  (top) and  $Re = 200$  (bottom).

## 5. CONCLUSIONS AND OUTLOOK

We investigated finite element formulations for a PPE reformulation of the incompressible Navier-Stokes equations. In the PPE reformulation, the momentum equation is in the form of a vector heat equation with electric boundary conditions, and the pressure appears as a global function of the velocity (obtained, at any time, as the solution to a Poisson equation). Thus this reformulation allows for high-order time-stepping via standard schemes. In particular, the decoupling of the velocity and the pressure can be achieved by IMEX time-stepping schemes, and modern high-order IMEX schemes can be applied in a straightforward manner.

We demonstrated via numerical examples that our proposed numerical schemes, based on the PPE reformulation (2.5–2.6), have the potential to achieve high-order both in space and in time, while avoiding severe time step restrictions. The methods have important advantages:

- (i) The use of an IMEX time-stepping strategy decouples the velocity and the pressure in the numerical methods, and at the same time avoids diffusive time step restrictions.
- (ii) The methods can achieve high-order in time with off-the-shelf high-order IMEX RK schemes. Therefore the code can be easily adapted to newly developed IMEX schemes with better properties, for instance, unconditional stability, order reduction avoidance, etc. A natural future research direction includes developing new IMEX RK time-stepping schemes for the PPE reformulations with such properties.
- (iii) Standard mixed finite element formulations of incompressible fluid flow problems (Stokes and Navier-Stokes equations) require the velocity and pressure approximations to satisfy the inf-sup condition for stability, which limits the choices of finite element approximations. Our new schemes allow for more flexible choices of finite element spaces for the velocity and pressure, avoiding the inf-sup condition.

Note also that an interesting feature of the methods studied in this paper is that the quantity  $\nabla \cdot \mathbf{u}$  converges to zero at an additional order relative to the accuracy of the velocity field itself. As a consequence, for well-resolved computations, the methodology will generally yield velocity fields that are extremely close to divergence-free, even though no discrete incompressibility principle needs to be imposed.

Despite the important advantages mentioned above, the methods also have some limitations:

- (i) The discretization of the (nonlinear) advection term is ad-hoc, and does not fit into the finite element formulation due to the discontinuities across elements in the tangential velocity. The current approach leads to convergent methods but results in degradations in the error convergence rates.
- (ii) The mixed formulation for the velocity deals with the EBC naturally. However, it introduces a saddle point problem. Therefore the choices for the FE approximations for  $\mathbf{u}$  and  $\sigma$  need to satisfy the inf-sup condition. The mixed formulation also increases the degrees of freedom of the discrete problem, as the new variable  $\sigma = \nabla \times \mathbf{u}$  is introduced.

#### APPENDIX A. DISCRETE SOLVABILITY OF THE POISSON EQUATION

The pressure Poisson problem (3.2) has pure Neumann boundary conditions prescribed, hence it is solvable only if a compatibility condition is satisfied (see Remark 2.1), and the solution is unique only up to an additive constant. In order to single out a unique solution, and at the same time to obtain a stable approximate solution in case the compatibility condition is not exactly satisfied (due to approximation errors), we employ the following standard least-squares approximation procedure. First, we impose an extra zero-mean constraint on the pressure:

$$\int_{\Omega} p \, dV = 0.$$

This gives rise to an augmented system for the pressure with an additional scalar variable representing the Lagrange multiplier for the zero-mean constraint. For simplicity, the presentation here is carried out for homogeneous boundary conditions  $\mathbf{g} = 0$ . The weak formulation then becomes: Find  $p \in H^1(\Omega)$  and  $c \in \mathbb{R}$  s.t.

$$(A.1a) \quad \langle \nabla p, \nabla q \rangle + \langle c, q \rangle = \langle \mathbf{f}, \nabla q \rangle - \nu \int_{\partial\Omega} \mathbf{n} \cdot (\nabla \times \sigma) q \, dS + \lambda \int_{\partial\Omega} (\mathbf{n} \cdot \mathbf{u}) q \, dS \quad \forall q \in H^1(\Omega),$$

$$(A.1b) \quad \langle p, d \rangle = 0 \quad \forall d \in \mathbb{R}.$$

Using standard nodal-based finite elements yields a linear system of the form

$$(A.2) \quad \begin{pmatrix} K & \mathbf{r} \\ \mathbf{r}^T & 0 \end{pmatrix} \cdot \begin{pmatrix} \mathbf{P} \\ c \end{pmatrix} = \begin{pmatrix} \mathbf{F} \\ 0 \end{pmatrix}.$$

Here  $K$  is the (symmetric) stiffness matrix of the FEM discretization of the Laplacian operator,  $\mathbf{r}$  is the vector corresponding to constant functions (the null-vector of  $K$ ),  $\mathbf{P}$  is the solution vector for the pressure  $p$ , and  $c$  is the Lagrange multiplier. While the stiffness matrix  $K$  is singular, the augmented matrix in (A.2) is nonsingular and it yields the following solution. Left-multiplying the equation  $K\mathbf{P} + c\mathbf{r} = \mathbf{F}$  by  $\mathbf{r}^T$  implies that  $c = (\mathbf{r}^T \mathbf{F}) / (\mathbf{r}^T \mathbf{r})$ , thus one has  $K\mathbf{P} = \text{proj}_{\mathcal{R}(K)} \mathbf{F}$ , where  $\mathcal{R}(K)$  is the range of  $K$ ; and  $\mathbf{r}^T \mathbf{P} = 0$  restricts that  $\mathbf{P} \in \mathcal{R}(K)$ .

Hence, the augmented system (A.1) addresses the two issues arising in solving the pressure Poisson equation: (i) it fixes the additive constant in  $p$  by choosing the zero-mean solution, and (ii) it ensures solvability, even when  $\nabla \cdot \mathbf{u} = 0$  is violated (see Remark 2.1), by projecting the right hand side  $\mathbf{F}$  to the range of  $K$ . Note that the augmented system (A.2) is similar to the one discussed in [28, 31, 55] where finite difference approaches are used.

#### ACKNOWLEDGMENT

The authors wish to acknowledge support by the National Science Foundation through the grants DMS-1719637 (Rosales), DMS-1719640 (Seibold and Zhou), and DMS-1719693 (Shirokoff). In addition, the authors received partial support through the grants DMS-1614043 (Rosales), and DMS-1318709 (Seibold and Zhou).

#### REFERENCES

- [1] I. Alonso-Mallo. Runge-Kutta methods without order reduction for linear initial boundary value problems. *Numer. Math.*, 91(4):577–603, 2002.
- [2] D. N. Arnold and H. Chen. Finite element exterior calculus for parabolic problems. *ESAIM Math. Model. Numer. Anal.*, 51(1):17–34, 2017.
- [3] D. N. Arnold, R. S. Falk, and J. Gopalakrishnan. Mixed finite element approximation of the vector Laplacian with Dirichlet boundary conditions. *Math. Models Methods Appl. Sci.*, 22(9):1250024, 2012.
- [4] D. N. Arnold, R. S. Falk, and R. Winther. Finite element exterior calculus, homological techniques, and applications. *Acta Numer.*, 15:1–155, 2006.
- [5] D. N. Arnold, R. S. Falk, and R. Winther. Finite element exterior calculus: From Hodge theory to numerical stability. *Bull. Amer. Math. Soc.*, 47(2):281–354, 2010.
- [6] U. M. Ascher, S. J. Ruuth, and Wetton B. T. R. Implicit-explicit methods for time-dependent partial differential equations. *SIAM J. Numer. Anal.*, 32(3):797–823, 1995.
- [7] U. M. Ascher, S. J. Ruuth, and R. J. Spiteri. Implicit-explicit Runge-Kutta methods for time-dependent partial differential equations. *Appl. Numer. Math.*, 25(2):151–167, 1997.
- [8] I. Babuška and J. Pitkäranta. The plate paradox for hard and soft simple support. *SIAM J. Math. Anal.*, 21(3):551–576, 1990.
- [9] I. Babuška. Stability of the domain with respect to the fundamental problems in the theory of partial differential equations, mainly in connection with the theory of elasticity, I, II. *Czechoslovak Math. J.*, 11(86):76–105, 1961.
- [10] J. B. Bell, P. Colella, and H. Glaz. A second-order projection method for the incompressible Navier-Stokes equations. *J. Comput. Phys.*, 85(2):257–283, 1989.
- [11] M. Benzi, G. H. Golub, and J. Liesen. Numerical solution of saddle point problems. *Acta Numer.*, 14:1–137, 2005.
- [12] S. C. Brenner, H. Li, and L.-Y. Sung. Multigrid methods for saddle point problems: Stokes and Lamé systems. *Numerische Mathematik*, 128(2):193–216, Oct 2014.
- [13] D. L. Brown, R. Cortez, and M. L. Minion. Accurate projection methods for the incompressible Navier-Stokes equations. *J. Comput. Phys.*, 168(2):464–499, 2001.
- [14] J. C. Butcher. Coefficients for the study of Runge-Kutta integration processes. *J. Austral. Math. Soc.*, 3(02):185–201, 1963.
- [15] M. H. Carpenter, D. Gottlieb, S. Abarbanel, and W.-S. Don. The theoretical accuracy of Runge-Kutta time discretizations for the initial boundary value problem: a study of the boundary error. *SIAM J. Sci. Comput.*, 16(6):1241–1252, 1995.
- [16] D. Cavaglieri and T. Bewley. Low-storage implicit/explicit Runge-Kutta schemes for the simulation of stiff high-dimensional ODE systems. *J. Comput. Phys.*, 286:172–193, 2015.
- [17] A. J. Chorin. Numerical solution of the Navier-Stokes equations. *Math. Comput.*, 22:745–762, 1968.
- [18] E. Erturk. Numerical solution of 2-D steady incompressible flow over a backward-facing step, part I: High Reynolds number solutions. *Comput. & Fluids*, 37:633–655, 2008.
- [19] M. Fortin and F. Brezzi. *Mixed and hybrid finite element methods*. Springer, New York, 1991.
- [20] C. Geuzaine and J.-F. Remacle. Gmsh: A 3-D finite element mesh generator with built-in pre-and post-processing facilities. *Int. J. Num. Meth. Eng.*, 79(11):1309–1311, 2009.
- [21] U. Ghia, K. N. Ghia, and C. T. Shin. High-Re solutions for incompressible flow using the Navier-Stokes equations and a multigrid method. *J. Comput. Phys.*, 48(3):387–411, 1982.
- [22] C. Greif, T. Rees, and D. B. Szyld. GMRES with multiple preconditioners. *SeMA J.*, 74:213–231, 2017.
- [23] P. M. Gresho and R. L. Sani. On pressure boundary conditions for the incompressible Navier-Stokes equations. *Int. J. Numer. Meth. Fluids*, 7:1111–1145, 1987.
- [24] J. L. Guermond and P. Mineev. High-order time stepping for the incompressible Navier-Stokes equations. *SIAM J. Sci. Comput.*, 37(6):A2656–A2681, 2015.
- [25] J. L. Guermond and P. Mineev. High-order time stepping for the Navier-Stokes equations with minimal computational complexity. *J. Comput. Appl. Math.*, 310:92–103, 2017.
- [26] J. L. Guermond, P. Mineev, and J. Shen. An overview of projection methods for incompressible flows. *Comput. Methods in Appl. Mech. Eng.*, 195(44–47):6011–6045, 2006.
- [27] F. H. Harlow and J. E. Welch. Numerical calculation of time-dependent viscous incompressible flow of fluid with a free surface. *Phys. Fluids*, 8:2182–2189, 1965.

- [28] W. D. Henshaw. A fourth-order accurate method for the incompressible Navier-Stokes equations on overlapping grids. *J. Comput. Phys.*, 113(6):13–25, 1994.
- [29] W. D. Henshaw and H.-O. Kreiss. Analysis of a difference approximation for the incompressible Navier-Stokes equations. Technical report, Los Alamos National Laboratory, 1995.
- [30] W. D. Henshaw, H.-O. Kreiss, and L. G. M. Reyna. A fourth-order accurate difference approximation for the incompressible Navier-Stokes equations. *Comput. Fluids*, 23(4):575–593, 1994.
- [31] W. D. Henshaw and N. A. Petersson. A split-step scheme for the incompressible Navier-Stokes equations. In M. M. Hafez, editor, *Numerical Simulation of Incompressible Flows*, volume 2502, pages 108–125. World Scientific, 2003.
- [32] M. Ignatova, G. Iyer, J. P. Kelliher, R. L. Pego, and A. D. Zarnescu. Global existence for two extended Navier-Stokes systems. *arXiv preprint arXiv:1308.4735*, 2013.
- [33] H. Johnston and J.-G. Liu. A finite difference method for incompressible flow based on local pressure boundary conditions. *J. Comput. Phys.*, 180(1):120–154, 2002.
- [34] H. Johnston and J.-G. Liu. Accurate, stable and efficient Navier-Stokes solvers based on explicit treatment of the pressure term. *J. Comput. Phys.*, 199(1):221–259, 2004.
- [35] U. Kangro and R. Nicolaides. Divergence boundary conditions for vector Helmholtz equations with divergence constraints. *ESAIM Math. Model. Numer. Anal.*, 33(3):479–492, 1999.
- [36] G. E. Karniadakis, M. Israeli, and S. Orszag. High-order splitting methods for the incompressible Navier-Stokes equations. *J. Comput. Phys.*, 97(2):414–443, 1991.
- [37] C. A. Kennedy and M. H. Carpenter. Additive Runge-Kutta schemes for convection-diffusion-reaction equations. *Appl. Numer. Math.*, 44(1):139–181, 2003.
- [38] J. Kim and P. Moin. Application of a fractional step method to incompressible Navier-Stokes equations. *J. Comput. Phys.*, 59:308–323, 1985.
- [39] R. C. Kirby. Algorithm 839: FIAT, a new paradigm for computing finite element basis functions. *ACM Trans. Math. Software*, 30(4):502–516, 2004.
- [40] R. C. Kirby. FIAT: Numerical construction of finite element basis functions. In Anders Logg, Kent-Andre Mardal, and Garth N. Wells, editors, *Automated Solution of Differential Equations by the Finite Element Method, Volume 84 of Lecture Notes in Computational Science and Engineering*, chapter 13, pages 247–255. Springer, Berlin, 2012.
- [41] L. Kleiser and U. Schumann. Treatment of the incompressibility and boundary conditions in 3-d numerical spectral simulation of plane channel flows. In E. H. Hirschel, editor, *Notes on Numerical Fluid Mechanics*, pages 165–173, Braunschweig, 1980. Proc. 3th GAMM Conf. on Numerical Methods in Fluid Mechanics, Vieweg.
- [42] T. Koto. IMEX Runge-Kutta schemes for reaction-diffusion equations. *J. Comput. Appl. Math.*, 215(1):182–195, 2008.
- [43] A. Krzywicki and O. A. Ladyzhenskaya. A grid method for the Navier-Stokes equations. *Dokl. Akad. Nauk SSSR*, 167:309–311, 1966.
- [44] W. Layton. *Introduction to the Numerical Analysis of Incompressible Viscous Flows*. Society for Industrial and Applied Mathematics, Philadelphia, PA, USA, 2008.
- [45] J.-G. Liu, J. Liu, and R. L. Pego. Stable and accurate pressure approximation for unsteady incompressible viscous flow. *J. Comput. Phys.*, 229(9):3428–2453, 2010.
- [46] A. Logg, K.-A. Mardal, G. N. Wells, et al. *Automated Solution of Differential Equations by the Finite Element Method*. Springer, Berlin, 2012.
- [47] J. B. Perot. An analysis of the fractional step method. *J. Comput. Phys.*, 108:51–58, 1993.
- [48] L. Rebholz and M. Xiao. Improved accuracy in algebraic splitting methods for Navier-Stokes equations. *SIAM J. Sci. Comput.*, 39(4):A1489–A1513, 2017.
- [49] D. Rempfer. On boundary conditions for the incompressible Navier-Stokes problems. *Appl. Mech. Rev.*, 59(3):107–125, 2006.
- [50] R. R. Rosales, B. Seibold, D. Shirokoff, and D. Zhou. Unconditional stability for multistep ImEx schemes: Theory. *SIAM J. Numer. Anal.*, 55(5):2336–2360, 2017.
- [51] R. R. Rosales, B. Seibold, D. Shirokoff, and D. Zhou. Spatial manifestations of order reduction in Runge-Kutta methods for initial boundary value problems. *arXiv preprint arXiv:1712.00897*, 2019.
- [52] R. Sani, J. Shen, O. Pironneau, and P. Gresho. Pressure boundary condition for the time-dependent incompressible Navier-Stokes equations. *Int. J. Numer. Methods Fluids*, 50(6):673–682, 2006.
- [53] J. M. Sanz-Serna, J. G. Verwer, and W. H. Hundsdorfer. Convergence and order reduction of Runge-Kutta schemes applied to evolutionary problems in partial differential equations. *Numer. Math.*, 50(4):405–418, 1986.
- [54] B. Seibold, D. Shirokoff, and D. Zhou. Unconditional stability for multistep ImEx schemes: Practice. *J. Comput. Phys.*, 376:295–321, 2019.
- [55] D. Shirokoff and R. R. Rosales. An efficient method for the incompressible Navier-Stokes equations on irregular domains with no-slip boundary conditions, high order up to the boundary. *J. Comput. Phys.*, 230(23):8619–8646, 2011.
- [56] R. Temam. Sur l’approximation de la solution des équations de Navier-Stokes par la méthode des pas fractionnaires, II. *Arch. Ration. Mech. Anal.*, 33(3):377–385, 1969.
- [57] J. G. Verwer. Convergence and order reduction of diagonally implicit Runge-Kutta schemes in the method of lines. In *Numerical Analysis*, pages 220–237, 1986.
- [58] Q. Zhang. GePUP: Generic projection and unconstrained PPE for fourth-order solutions of the incompressible Navier-Stokes equations with no-slip boundary conditions. *J. Sci. Comput.*, 67(3):1134–1180, Jun 2016.
- [59] D. Zhou, B. Seibold, D. Shirokoff, P. Chidyagwai, and R. R. Rosales. Meshfree finite differences for vector poisson and pressure Poisson equations with electric boundary conditions. In M. Griebel and M. A. Schweitzer, editors, *Meshfree*

*methods for Partial Differential Equations VII*, volume 100 of *Lecture Notes in Computational Science and Engineering*, pages 223–246. Springer, 2015.

DEPARTMENT OF MATHEMATICS, MASSACHUSETTS INSTITUTE OF TECHNOLOGY, 77 MASSACHUSETTS AVENUE, CAMBRIDGE, MA 02139

*E-mail address:* `rrr@math.mit.edu`

DEPARTMENT OF MATHEMATICS, TEMPLE UNIVERSITY, 1805 NORTH BROAD STREET, PHILADELPHIA, PA 19122

*E-mail address:* `seibold@temple.edu`

*URL:* `http://www.math.temple.edu/~seibold`

DEPARTMENT OF MATHEMATICAL SCIENCES, NEW JERSEY INSTITUTE OF TECHNOLOGY, UNIVERSITY HEIGHTS, NEWARK, NJ 07102

*E-mail address:* `david.g.shirokoff@njit.edu`

*URL:* `http://web.njit.edu/~shirokof`

DEPARTMENT OF MATHEMATICS, CALIFORNIA STATE UNIVERSITY, LOS ANGELES, 5151 STATE UNIVERSITY DRIVE, LOS ANGELES, CA 90032

*E-mail address:* `dong.zhou@calstatela.edu`